PFE / Master 2 Internship

Field of Study: Optimisation, Recherche Opérationnelle, Commande (ENSTA)
Master Optimization (Université Paris-Saclay)
Scholar Year: 2015-2016

Stabilization and analysis of stick-slip phenomena in oil-drilling facilities

Confidentiality Notice
Non-confidential report and publishable on Internet

Author:
BONNET Benoît

Promotion:
2016

ENSTA ParisTech Tutor:
JEAN Frédéric

Advisor/supervisor:
DI-MEGLIO Florent

Internship from 04/04/2016 to 31/07/2016

Name of the host organism: CAS, École Nationale Supérieure des Mines de Paris
Address: 60 Boulevard Saint-Michel, 75006 Paris

Confidentiality Notice

This present document is not confidential. It can be communicated outside in paper format or distributed in electronic format.

Acknowledgment

I would like to thank in the first place Florent Di Meglio for supervising me throughout this internship and for allowing me to work on this interesting research topic. My thanks also go to Delphine Bresch-Pietri for her advices and guidance.

I would like to thank my employer ARMINES as well as the members of the Centre d'Automatique et Systèmes of École Nationale des Mines de Paris for hosting me during these 4 months.

As always, I would like to thank dearly Frédéric Jean who profoundly inspired me during the three years I spent studying at ENSTA. I would also like to extend my gratitude to Filippo Santambrogio, the head of my master program, for his constant presence and care for his students.

I would like to thank my family for their kind support and for their constant encouragements, with a special thought for my father who constantly helped and motivated me throughout my years of higher education.

I send the dearest attentions to my partner Élise and my friends who are one of the main fuels driving my life.

Abstract

The coming work aims at presenting new results obtained in the field of control of oil drilling facilities. The theoretical part of our work is mainly based on *backstepping controller design*, a PDE-inspired technique developped a decade ago by Krstic and Smyshlyaev which allows to conduct Lyapunov stability analyses on a wide classe of dynamical systems. The main novelties of this work are to consider the presence of non-linear interactions between the driller and the rock and the main practical issues they generate (parts of the dynamics being too fast for the actuators to be exactly compensated and impossibility to carry out a prediction approach on the disturbances) in the backstepping controller design. In this framework, we generalized a stability result obtained in the linear case by Di Meglio & Bresch-Pietri to a more general *Input to State Stability* result in order to theoretically justify the controller design we perform. To this end, we first conveyed a precise analysis of the *stick-slip limit cycle* arising in the dynamics in order to include a well chosen averaged value in the controller design. Both these theoretical results and the physical peculiarities of the models of drilling systems we discuss are supported by figures obtained from a Matlab simulator which implementation is also exposed.

Contents

List of Figures

Introduction

The modelling and dynamical study of oil drilling systems has been the subject of an active investigatin by a wide community for several decades. Be it in industry, mechanics or applied mathematics, these systems present many compelling challenges and technical difficulties and are still the object of a constant focus.

Due to recent developments in control theory, more profound studies were possible for such systems from a mathematical point of view (see for instance [2]). And for good reason, said systems do involve complex issues pertaining to dealing with delayed and non-linear systems, boundary control of PDEs, observers design, robustness analysis, etc...

Our work with Florent Di Meglio and Delphine Bresch-Pietri mainly focuses on understanding and controlling the so-called *stick-slip phenomenon* arising in rotary drilling structures. As we shall describe it more precisely in section I.1, a rotary drilling structure is the concatenation of different kinds of pipes at the end of which is fixed a drilling bit. This bit digs through the soil by means of several vertical cutting blades (see figure I.1 for more details).

A common phenomenon occurring in the drilling procedure is that the bit sticks and remains still because a too big quantity of rock stacks in front of the blades, generating important friction forces. This leads to an accumulation of torsional and axial constraints in the pipes that are unleashed with a violent velocity burst when the system has stored enough energy to overcome the resistance of the rock. This kind of situation is very harmful to the system, it reduces its efficiency and greatly damages its parts (pipes, bit, etc...). Thus, the design of control strategies preventing this hazard from arising is a central issue in the field of oil drilling industry.

Designing control laws for this kind of system is rather complicated. If the bottom hole assembly (*BHA*) to which the bit is attached is modeled as a lump mass for instance, controlling the system goes down to controlling a non-linear differential equation with distributed state delays using only delayed controls. Indeed, said controls can only be applied at the surface to be then transported by the pipes at finite speed. Recent work done by Delphine Bresch-Pietri and Florent Di Meglio was dedicated to the design of this type of controller (see [3]) for a linear lump BHA model. Describing this design will be done in Section IV.3 and will be of great importance for our developments.

The work we did with Florent Di Meglio is linked to another pratical issue arising in the stick-slip cycles of rotary drilling systems. The stick-slip phenomenon can occur for both axial and angular displacements, but the frequency of the axial stick-slip cycle is in practice way larger than the torsional oscillations' one, making it impossible for a realistic actuator to compensate or control them accurately. We were thus interested in the influence of controlling the torsional oscillations of the system - which is possible in practice - and to see what consequences it had on the axial limit cycle. The main contributions of my work consisted in the three following points along with an extensive reading of articles dealing with backstepping control :

(i) Implementing two simulators in Matlab describing the drilling system using either a *lump* or a *distributed* model for the dynamics of the BHA. The implementation of the simulator in the lump framework being the most relevant for our work, it is detailed in Chapter II.

(ii) Conveying a detailed semi-analytical study of the axial stick-slip cycle arising from the incorporation of non-linear friction terms in our model as developped in Chapter III in order to design a more accurate controller. Further computation details are given in appendix A.

(iii) Extending a Lyapunov-based stability result obtained in [3] - in the framework of a lump BHA model - to a more general result of *Input to State Stability* (see [4] for a precise description of the notion). This result along with the design of the corresponding controllers is detailed in Chapter IV.

Part I

Mathematical model of a rotary drilling system and introduction to the main control issues

I.1 Physical description of the drilling system

In this first section, we shall describe the physics of a rotary oil-drilling system. We will mainly stick to the descriptions of the facilities given in [1], but in a simplified way since all the mechanical parts of the machinery are not of interest in our work.

In this simplified framework, a rotary system can be described (see figure I.1 below) as the combination of cables, the *drillpipes*, connected at the surface to a *rotary table* and at the bottom to the so-called *bottom hole assembly* (hereafter referred to as BHA) on which is fixed the *drillbit*.

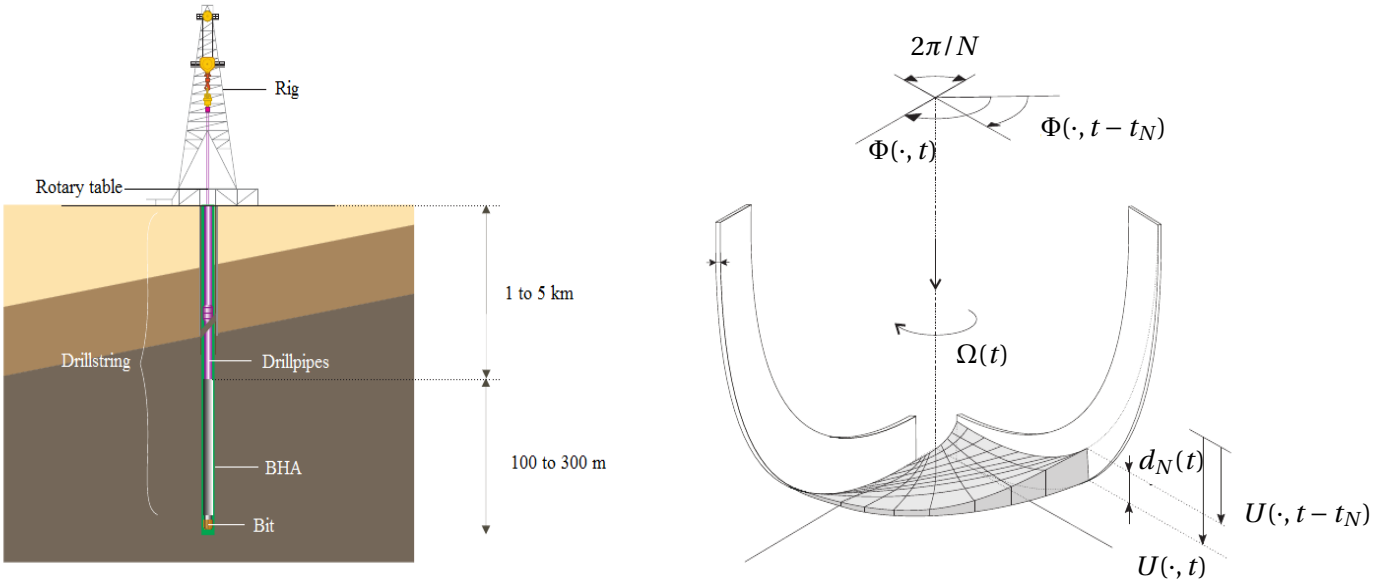

Figure I.1: *Schematic view of the drilling structure (left) and of the drillbit (right) extracted from [1]*

To be slightly more precise, as well as for introducing some of the physical parameters governing the dynamics of the system :

- The drillpipes are cables of length L_p and area A_p that are assumed to undergo purely longitudinal and torsional motions, and the system is assumed to be fixed along the orthogonal direction to the vertical axis [1].

[1] In practice, horizontal vibrations do arise in this type of drilling system, but they are mostly considered as being a consequence

- The BHA consists of pipes made of heavier material, of length L_b, total area A_b and total mass M_b. This part of the system will be of great interest for our two models since it is the one making the junction between the upper part of the system and the drillbit.

- The rotary table at the surface drives the system by imposing a weight $W_{\text{op}}(\cdot)$ and a torque $T_{\text{op}}(\cdot)$ to the drillpipes. The drillpipes then transmit said weight and torque to the BHA which acts directly on the drillbit.

- The drillbit is a cylindrical structure of radius a composed of N cutting blades spaced regularly by an angle $\frac{2\pi}{N}$ (see figure I.1 on the right).

The thickness of the rock ridge in front of a blade, equal to $d_N(\cdot) = \frac{d(\cdot)}{N}$ and the time period $t_N(\cdot)$ taken by the bit to rotate of an angle $\frac{2\pi}{N}$ are both crucial to describing the dynamics of the system as we shall see in the next section. They are defined as follows

$$\forall\, t \in \mathbb{R}_+ \ , \quad \begin{cases} U(L,t) - U(L,t-t_N) = d_N(t) \\ \Phi(L,t) - \Phi(L,t-t_N) = \dfrac{2\pi}{N} \end{cases} \tag{I.1}$$

where the functions $U(\cdot,\cdot)$ and $\Phi(\cdot,\cdot)$ are respectively the axial and torsional displacements of the system $\{\text{drillpipes}\} \cup \{\text{BHA}\}$ which total length is $L = L_p + L_b$.

These two terms, defined implicitly and requiring knowledge of the history of the system, will appear explicitly in the dynamics of the drilling system. One can see here that the system will *intrisically* involve delayed terms that cannot be neglected or compensated afterwards as it is usually done in automatics for mildly delay systems.

I.2 Mathematical models for the pipes and bit-rock interaction

Now that we have presented the physical system which we are interested in during the coming development, let us describe the mathematical model that we mainly considered for its dynamics. The two mains approaches that are known to be considered for modelling an oil-drilling system are both about the BHA model which will be described more in detail in section I.3.

Yet before considering the model chosen for the dynamics of the BHA, which will consists the main originality of our model-choice, let us discuss the behaviour of the other parts of the system.

I.2.1 Drillpipes model

Propagation equations

The drillpipes are modeled as one dimensional rods that undergo axial and torsional motions. Said motions are described through wave propagation equations of respective velocities c_ξ for the axial displacement $(x,t) \mapsto U(x,t)$ and c_ϕ for the angular displacements $(x,t) \mapsto \Phi(x,t)$.

The wave propagation within the pipes then follows the equations

$$\forall (x,t) \in [0, L_p] \times \mathbb{R}_+ \ , \quad \begin{cases} \dfrac{\partial^2 U}{\partial t^2}(x,t) - c_\xi^2 \dfrac{\partial^2 U}{\partial x^2}(x,t) = -g \\ \dfrac{\partial^2 \Phi}{\partial t^2}(x,t) - c_\phi^2 \dfrac{\partial^2 \Phi}{\partial x^2}(x,t) = 0 \end{cases} \tag{I.2}$$

where g is the gravity.

The topside boundary conditions for these equations can be given in several forms depending on the type of models considered for the action of the rotary table.

of the axial and torsional vibrations more than a self-excited phenomenon

Rotary table boundary conditions

The nature of the boundary conditions imposed at the rotary table will have a great influence on the qualitative behaviour of the open-loop solutions of the system.

For the axial components, we always assume that the user prescribes a weight at the rotary table, namely

$$\frac{\partial U}{\partial x}(0,t) = -W_{\text{op}}(t) \tag{I.3}$$

For the torsional components, several models can be considered. The simplest one is to assume that the user applies directly a rotation speed on the system (as is to done for instance in [1]). This condition reads

$$\frac{\partial \Phi}{\partial t}(0,t) = -\Omega_{\text{op}}(t) \tag{I.4}$$

This condition however is not fully realistic. In pratice, the user imposes a torque on the system and the condition reads

$$\frac{\partial \Phi}{\partial x}(0,t) = -T_{\text{op}}(t) \tag{I.5}$$

A possible refinement of this condition would be to add an actuator dynamics to the rotary table. We shall describe this particular feature later on.

I.2.2 Bit-rock interaction

Another important part of the description of the dynamics that will not depend on the model chosen for the BHA is the bit-rock interaction. A detailed description of said interactions can be found in most of the main mechanics articles dealing with the modelling of drilling systems (see for instance [1] or [5]).

For the sake of brevity and simplicity we shall only give short descriptions and explanations in this section, the exact physical details of the model being of lesser importance for us than its mathematical properties.

The bit-rock interaction is composed of a weight-on-bit W and a torque-on-bit T. Both can be described by being separated into two contributions as we detail in the paragraphs I.2.2 and I.2.2.

Cutting forces

The first type of contributions is made of *cutting* forces denoted by (W_c, T_c), accounting for the sum of the forces applied by the rock on the blades of the bit while a cutting action is performed.

This action is assumed to be proportional to the depth of cut $d(\cdot)$ introduced in equation (I.1) and thus implicitly involves the rotation time $t_N(\cdot)$.

$$\forall\, t \in \mathbb{R}_+ \,,\ \begin{cases} W_c(t) = a\zeta\epsilon d(t) = a\zeta\epsilon N\left[U(t) - U(t-t_N)\right] \\ T_c(t) = \dfrac{1}{2}a^2\epsilon d(t) = \dfrac{1}{2}a^2\epsilon N\left[U(t) - U(t-t_N)\right] \end{cases} \tag{I.6}$$

where ζ and ϵ are physical parameters describing the material.

Friction forces

The second type of contribution is made of *friction* forces denoted by (W_f, T_f), accounting for the frictional contacts of the bit with the rock.

The definition of these terms is less intuitive than for the cutting ones. They are supposed to take place only when the bit is in an *axial stick-phase*, namely when the axial velocity of the bit vanishes. We recall that this situation occurs when the bit has dug too deep inside the rock, the height of rock in front of the blades preventing it to turn properly.

When this phase is reached, the frictional forces become positive and compensate exactly the other forces so that the bit stays at axial equilibrium. The system will remain in said equilibrium as long as the cutting forces do not overcome the frictional process. When they do, the system enters a new *slip-phase*.

These efforts are taken proportional to a discontinuous function $G(\cdot)$ defined by

$$G[V(t)] = \begin{cases} 0 & \text{if } V(t) > 0 \\ \tilde{G}(t) & \text{if } V(t) \leq 0 \end{cases} \tag{I.7}$$

where $\tilde{G}(\cdot)$ is chosen so as to cancel the axial dynamics as mentioned before.

The friction contributions of the system read

$$\forall\, t \in \mathbb{R}_+ \,,\ \begin{cases} W_f(t) = -\lambda G[V(t)] \\ T_f(t) = -\lambda\beta G[V(t)] \end{cases} \tag{I.8}$$

where λ and β are physical parameters of the model.

These friction efforts are the terms in the dynamics that induce the axial limit cycle. Whenever the bit axially sticks, the function $G[V(\cdot)]$ goes from 0 to a given positive value, remains at a plateau, and then decreases slowly as the system stores energy to overcome the frictional process and enter a new slip phase. This behaviour will be described in ample details in section **??** dedicated to the mathematical analysis of the axial limit cycle.

Let it be noted here that a similar function could also be introduced in order to model the *torsional stick-phases* of the system. We will not however use it in our model since torsional stick seldom occurs, unlike axial stick that is empirically reached very quickely by the system for almost any realistic configuration as it will be explained in the paragraph II.2.2.

Besides, as it will be explained later, we will aim at stabilizing the torsional dynamics of the system around its nominal value, making it useless to take into account the torsional stick phenomenon occurring when the torsional velocity vanishes.

I.3 Mathematical model for the BHA

Now that we have described the models for the other components of the system, let us discuss the BHA models. As mentioned before, there are two classical ways of modeling a BHA from a mathematical point of view :

- ◇ Describing the BHA as a rigid body on which one applies Newton's laws in order to derive its governing equations. This model is refered to as a *lump* BHA model.
- ◇ Describing the BHA as a continuous, deformable solid into which wave propagation occurs. This model is refered to as a *distributed* BHA model.

The model which we used for our work is the lump BHA model. It allows more profound analytical considerations and fits well into the framework of delay systems. I also implemented numerically the distributed BHA model, but its description is not relevant in the framework of our study so it will not be presented in the framework of this report.

I.3.1 Dynamics of the BHA

We recall that the axial and angular displacements of the system write $U(\cdot,\cdot)$ and $\Phi(\cdot,\cdot)$. In particular, the axial and angular displacement of the BHA write $(U(L_p,\cdot)$ and $\Phi(L_p,\cdot)$.

Applying Newton's third law to the BHA yields

$$\begin{cases} M_b \dfrac{\partial^2 U}{\partial t^2}(L_p,t) = M_b g - EA_p \dfrac{\partial U}{\partial x}(L_p,t) - W_c(t) - W_f(t) \\ I_b \dfrac{\partial^2 \Phi}{\partial t^2}(L_p,t) = -GJ_p \dfrac{\partial \Phi}{\partial x}(L_p,t) - T_c(t) - T_f(t) \end{cases} \tag{I.9}$$

where g is the gravity, A_p and J_p are the surface and polar moment of inertia of the drillpipes, I_b is the moment of inertia of the BHA, E its Young modulus and G its shear modulus

The $\frac{\partial}{\partial x}$ terms denote the forces exerced by the pipes on the BHA. The other terms are defined in the paragraph I.2.2 and account for the bit-rock interaction.

It is possible to compute the steady state solution associated to (I.2) using (I.9) and (I.5) as boundary conditions. This form of this solution is

$$\forall (x,t) \in [0,L_p] \times \mathbb{R}_+ \ , \ \bar{U}(x,t) = V_0 t + U_s(x) \ \ , \ \ \bar{\Phi}(x,t) = \Omega_0 t + \Phi_s(x) \tag{I.10}$$

where (V_0, Ω_0) are the reference axial and angular velocities of the system [2].

$U_s(\cdot)$ and $\Phi_s(\cdot)$ are easy to compute by plugging the expressions (I.10) into (I.2), (I.5) and (I.9). The reference trajectories are then given by

$$\begin{cases} \bar{U}(x,t) = V_0 t - \dfrac{\bar{W}_{\text{op}}}{EA_p} x + \dfrac{\rho g}{2E} x^2 \\ \bar{\Phi}(x,t) = \Omega_0 t - \dfrac{\bar{T}_{\text{op}}}{GJ_p} x \end{cases} \tag{I.11}$$

where $(\bar{W}_{\text{op}}, \bar{T}_{\text{op}})$ are the nominal weight-on-bit and torque-on-bit chosen so as to cancel drift terms in the dynamics. This steady solution is associated to the corresponding steady delay $\bar{t}_N = \frac{2\pi}{N\Omega_0}$.

I.3.2 Dynamics of the error with respect to the nominal trajectory

We will be interested in the remainder of our work not directly in equations (I.9) but rather in the equation describing the dynamics of the error variables defined as follows

$$\forall (x,t) \in [0,L] \times \mathbb{R}_+ \ , \ \ \tilde{U}(x,t) = U(x,t) - \bar{U}(x,t) \ \ , \ \ \tilde{\Phi}(x,t) = \Phi(x,t) - \bar{\Phi}(x,t) \ \ , \ \ \tilde{t}_N(t) = t_N(t) - \bar{t}_N \tag{I.12}$$

Using the expression of the steady state solution as well as the expression for the bit-rock interaction described in the paragraph I.2.2 through the equations (I.6) and (I.8), one gets the following equations for the error-dynamics of the BHA

$$\begin{cases} M_b \dfrac{\partial^2 \tilde{U}}{\partial t^2}(L_p,t) = -EA_p \dfrac{\partial \tilde{U}}{\partial x}(L_p,t) - a\zeta\epsilon N \left[\tilde{U}(L_p,t) - \tilde{U}(L_p, t-\bar{t}_N - \tilde{t}_N(t))\right] \\ \qquad\qquad - a\zeta\epsilon N V_0 \tilde{t}_N(t) + \lambda a\zeta\epsilon N g \left[\dfrac{\partial \tilde{U}}{\partial t}(L_p,t)\right] \\ I_b \dfrac{\partial^2 \tilde{\Phi}}{\partial t^2}(L_p,t) = -GJ_p \dfrac{\partial \tilde{\Phi}}{\partial x}(L_p,t) - \dfrac{a^2}{2}\epsilon N \left[\tilde{U}(L_p,t) - \tilde{U}(L_p, t-\bar{t}_N - \tilde{t}_N(t))\right] \\ \qquad\qquad - \dfrac{a^2}{2}\epsilon N V_0 \tilde{t}_N(t) + \lambda\beta \dfrac{a^2}{2}\epsilon N g \left[\dfrac{\partial \tilde{U}}{\partial t}(L_p,t)\right] \end{cases} \tag{I.13}$$

where the delay error $\tilde{t}_N(\cdot)$ can be expressed as the solution of an implicit equation by injecting its expression given in (I.12) in (I.1), namely

$$\left[\tilde{\Phi}(L_p,t) - \tilde{\Phi}(L_p, t-\bar{t}_N - \tilde{t}_N(t))\right] + \Omega_0 \tilde{t}_N(t) = 0 \tag{I.14}$$

However in practice, the only measurements which are available to a user are velocity measurements. Let us rewrite these equations as functions of $V(\cdot) = \frac{\partial \tilde{U}}{\partial t}(L_p,\cdot)$, $\Omega(\cdot) = \frac{\partial \tilde{\Phi}}{\partial t}(L_p,\cdot)$

$$\begin{cases} M_b \dot{V}(t) = -EA_p \dfrac{\partial \tilde{U}}{\partial x}(L_p,t) - a\zeta\epsilon N \displaystyle\int_{t-\bar{t}_N-\tilde{t}_N(t)}^{t} V(s)\mathrm{d}s - a\zeta\epsilon N V_0 \tilde{t}_N(t) + \lambda a\zeta\epsilon N g\left[V(t)\right] \\ I_b \dot{\Omega}(t) = -GJ_p \dfrac{\partial \tilde{\Phi}}{\partial x}(L_p,t) - \dfrac{a^2}{2}\epsilon N \displaystyle\int_{t-\bar{t}_N-\tilde{t}_N(t)}^{t} V(s)\mathrm{d}s - \dfrac{a^2}{2}\epsilon N V_0 \tilde{t}_N(t) + \lambda\beta\dfrac{a^2}{2}\epsilon N g\left[V(t)\right] \\ \displaystyle\int_{t-\bar{t}_N-\tilde{t}_N(t)}^{t} \Omega(s)\mathrm{d}s + \Omega_0 \tilde{t}_N(t) = 0 \end{cases} \tag{I.15}$$

A few remaining last steps are necessary for us to arrive at the master equations that were the main interest of our work.

[2] In this report, all the quantities denoted with a "0" subscript will conventionally refer to nominal values.

I.3.3 Hyperbolic formalism and Riemann variables

For our purpose, it is more convenient to consider an alternative set of variables in order to describe the wave propagation phenomena occurring in the system. Let us define the so-called *Riemann variables*, noted here (u, v, ϕ, ψ), by

$$u = \frac{\partial \tilde{U}}{\partial t} - c_\xi \frac{\partial \tilde{U}}{\partial x} \ , \ v = \frac{\partial \tilde{U}}{\partial t} + c_\xi \frac{\partial \tilde{U}}{\partial x} \ , \ \phi = \frac{\partial \tilde{\Phi}}{\partial t} - c_\phi \frac{\partial \tilde{\Phi}}{\partial x} \ , \ \psi = \frac{\partial \tilde{\Phi}}{\partial t} + c_\phi \frac{\partial \tilde{\Phi}}{\partial x} \tag{I.16}$$

where we dropped the space and time explicit dependence for conciseness.

These variables allow us to rewrite the wave propagation equations (I.2) in the form

$$\forall (x,t) \in [0, L_p] \times \mathbb{R}_+ \ , \ \begin{cases} \dfrac{\partial u}{\partial t}(x,t) + c_\xi \dfrac{\partial u}{\partial x}(x,t) = 0 \\ \dfrac{\partial v}{\partial t}(x,t) - c_\xi \dfrac{\partial v}{\partial x}(x,t) = 0 \end{cases} \ , \ \begin{cases} \dfrac{\partial \phi}{\partial t}(x,t) + c_\phi \dfrac{\partial \phi}{\partial x}(x,t) = 0 \\ \dfrac{\partial \psi}{\partial t}(x,t) - c_\phi \dfrac{\partial \psi}{\partial x}(x,t) = 0 \end{cases} \tag{I.17}$$

Physically speaking, this decomposition accounts for the fact that the propagation of a wave along a given axis can alternatively be described as a super-imposition of two one-directional waves travelling along said axis in opposite directions with no coupling except at the boundaries.

This decomposition is also convenient for writing the continuity of velocities at the interface between the pipes and the BHA. Indeed

$$\begin{cases} \dfrac{\partial \tilde{U}}{\partial t}(L_p, t) = V(t) \iff v(L_p, t) = -u(L_p, t) + 2V(t) \\ \dfrac{\partial \tilde{\Phi}}{\partial t}(L_p, t) = \Omega(t) \iff \psi(L_p, t) = -\phi(L_p, t) + 2\Omega(t) \end{cases} \tag{I.18}$$

as well as for expressing the terms $\frac{\partial \tilde{U}}{\partial x}$ and $\frac{\partial \tilde{\Phi}}{\partial x}$ as functions of the downward-propagating waves (u, ϕ) and of the state of the BHA (V, Ω) through

$$\frac{\partial \tilde{U}}{\partial x}(L_p, t) = \frac{1}{c_\xi}\left[V(t) - u(L_p, t)\right] \ , \ \frac{\partial \tilde{\Phi}}{\partial x}(L_p, t) = \frac{1}{c_\phi}\left[\Omega(t) - \phi(L_p, t)\right] \tag{I.19}$$

This enables us to write the master equations of the dynamics of the BHA around its nominal trajectory as

$$\begin{cases} \dot{V}(t) = \dfrac{EA_p}{M_b c_\xi}\left[u(L_p,t) - V(t)\right] - \dfrac{a\zeta\epsilon N}{M_b} \displaystyle\int_{t-\tilde{t}_N-\tilde{t}_N(t)}^{t} V(s)\mathrm{d}s - \dfrac{a\zeta\epsilon N}{M_b} V_0 \tilde{t}_N(t) + \lambda \dfrac{a\zeta\epsilon N}{M_b} g\left[V(t)\right] \\ \dot{\Omega}(t) = \dfrac{GJ_p}{I_b c_\phi}\left[\phi(L_p,t) - \Omega(t)\right] - \dfrac{a^2\epsilon N}{2I_b} \displaystyle\int_{t-\tilde{t}_N-\tilde{t}_N(t)}^{t} V(s)\mathrm{d}s - \dfrac{a^2\epsilon N}{2I_b} V_0 \tilde{t}_N(t) + \lambda\beta \dfrac{a^2\epsilon N}{2I_b} g\left[V(t)\right] \\ \displaystyle\int_{t-\tilde{t}_N-\tilde{t}_N(t)}^{t} \Omega(s)\mathrm{d}s + \Omega_0 \tilde{t}_N(t) = 0 \end{cases} \tag{I.20}$$

There now remains to put these equations into non-dimensional form.

Remark. From a control perspective, working in the decoupled hyperbolic framework is all the more convenient since it allows to split the wave propagation into :

- the components (u, ϕ) going from the rotary table to the BHA which can be controlled by the user through the application of boundary inputs.

- the components (v, ψ) going from the BHA to the rotary table which are driven by the dynamics of the BHA (see (I.18)).

I.4 Non-dimensionalization of the system of equations

The last step in our modeling of the system is to introduce non-dimensional variables and parameters.

We will proceed to non-dimensionalize our system using the following scaling parameters denoted by the index $\bullet_*$:

$$t_* = \frac{2\pi}{\omega_1} = 2\pi\sqrt{\frac{3I_b + I_p}{3C_p}} \quad , \quad L_* = L_p \quad , \quad d_* = \frac{2C_p}{\epsilon a^2} \quad , \quad T_* = \frac{1}{2}\epsilon a^2 d^* \quad , \quad W_* = \zeta a \epsilon d^* \tag{I.21}$$

where $C_p = \frac{GJ_p}{L_p}$ is the global torsional stiffness of the pipes. We also define the new non-dimensional variables

$$\chi = \frac{x}{L_*} \quad , \quad \tau = \frac{t}{t_*} \quad , \quad z(\tau) = \frac{t_*}{d_*} V(t_*\tau) \quad , \quad \omega(\tau) = t_*\Omega(t_*\tau) \quad , \quad \tilde{\tau}_N(\tau) = t_*\tilde{t}_N(t_*\tau) \tag{I.22}$$

By abuse of notation, we refer from now on to the non-dimensional Riemann variables using $\tilde{\bullet}$ notations.

We also introduce the non-dimensional parameters associated to the bit

$$v_0 = \frac{t_*}{d_*} V_0 \quad , \quad \omega_0 = t_*\Omega_0 \tag{I.23}$$

Using these variables and coefficents, we can rewrite our complete cascaded ODE-PDE system in non-dimensional form as follows for all $(\chi,\tau) \in [0,1]\times\mathbb{R}_+$

$$\begin{array}{l}
\text{Drillpipes dynamics} \left\{ \begin{array}{l}
\dfrac{\partial \tilde{u}}{\partial \tau}(\chi,\tau) + \dfrac{t_*}{L_*} c_\xi \dfrac{\partial \tilde{u}}{\partial \chi}(\chi,\tau) = 0 \\
\dfrac{\partial \tilde{v}}{\partial \tau}(\chi,\tau) - \dfrac{t_*}{L_*} c_\xi \dfrac{\partial \tilde{v}}{\partial \chi}(\chi,\tau) = 0 \\
\dfrac{\partial \tilde{\phi}}{\partial \tau}(\chi,\tau) + \dfrac{t_*}{L_*} c_\phi \dfrac{\partial \tilde{\phi}}{\partial \chi}(\chi,\tau) = 0 \\
\dfrac{\partial \tilde{\psi}}{\partial \tau}(\chi,\tau) - \dfrac{t_*}{L_*} c_\phi \dfrac{\partial \tilde{\psi}}{\partial \chi}(\chi,\tau) = 0
\end{array} \right. \quad \text{Boundary conditions} \left\{ \begin{array}{l}
\tilde{u}(0,\tau) = \tilde{v}(0,\tau) + 2P_{\text{ax}}\tilde{w}_{\text{op}} \\
\tilde{\phi}(0,\tau) = \tilde{\psi}(0,\tau) + 2P_{\text{tor}}\tilde{t}_{\text{op}} \\
\tilde{v}(1,\tau) = -\tilde{u}(1,\tau) + 2z(\tau) \\
\tilde{\psi}(1,\tau) = -\tilde{\phi}(1,\tau) + 2\omega(\tau)
\end{array} \right. \\
\text{BHA dynamics} \left\{ \begin{array}{l}
\dfrac{\mathrm{d}z}{\mathrm{d}\tau}(\tau) = c_0^z\left[\tilde{u}(1,\tau) - z(\tau)\right] - c_1 \displaystyle\int_{\tau-\tilde{\tau}_N-\tilde{\tau}_N}^{\tau} z(s)\mathrm{d}s - c_2\tilde{\tau}_N(\tau) + c_1\lambda g\left[z(\tau)\right] \\
\dfrac{\mathrm{d}\omega}{\mathrm{d}\tau}(\tau) = c_0^\omega\left[\tilde{\phi}(1,\tau) - \omega(\tau)\right] - c_3 \displaystyle\int_{\tau-\tilde{\tau}_N-\tilde{\tau}_N}^{\tau} z(s)\mathrm{d}s - c_4\tilde{\tau}_N(\tau) + c_3\lambda\beta g\left[z(\tau)\right] \\
\displaystyle\int_{\tau-\tilde{\tau}_N-\tilde{\tau}_N}^{\tau} \omega(s)\mathrm{d}s + \omega_0\tilde{\tau}_N(\tau) = 0
\end{array} \right.
\end{array} \tag{I.24}$$

where

$$\left\{ \begin{array}{lll}
c_0^z = \dfrac{EA_p t_*}{M_b c_\xi} & , \quad c_1 = \dfrac{a\zeta\epsilon N t_*^2}{M_b} & , \quad c_2 = \dfrac{a\zeta\epsilon N V_0 t_*^3}{M_b d_*} \\
c_0^\omega = \dfrac{GJ_p t_*}{I_b c_\phi} & , \quad c_3 = \dfrac{a^2\epsilon N d_* t_*^2}{2I_b} & , \quad c_4 = \dfrac{a^2\epsilon N d_* V_0 t_*^3}{2I_b} \\
P_{\text{ax}} = \dfrac{2c_\xi t_* W_*}{EA_p d_*} & , \quad P_{\text{tor}} = \dfrac{2c_\phi t_* T_*}{2GJ_p d_*} &
\end{array} \right. \tag{I.25}$$

and $g(\bullet)$ is defined by

$$\forall \tau \in \mathbb{R}_+ \ , \quad g[z(\tau)] = \begin{cases} 0 & \text{if } z(\tau) > -v_0 \\ \tilde{g}(\tau) & \text{if } z(\tau) \le -v_0 \end{cases} \tag{I.26}$$

where $\tilde{g}(\cdot)$ is a function which cancels the axial dynamics. This choice of model will be explained in paragraph II.1.2.

Now that we derived the mathematical model for our system, the next chapter will be dedicated to the Matlab implementation of the simulator and to describing the dynamical features of the system in order to highlight the main control issues we dealt with.

Part II

Structure of the simulator and introduction to the main control issues

II.1 Details of the implementation of a Matlab simulator for the lump BHA model

Implementing a simulator in Matlab constituted a significant part of my work. In retrospect, it does not seem that much of a challenge anymore, but it took a few complete rewritings as well as a great deal of care in the layouts of the code. The purpose of this simulator is to model the system of equations (I.24) as accurately as possible and taking into account all of its intricacies and couplings. Its overall structure can be represented using the following flowchart.

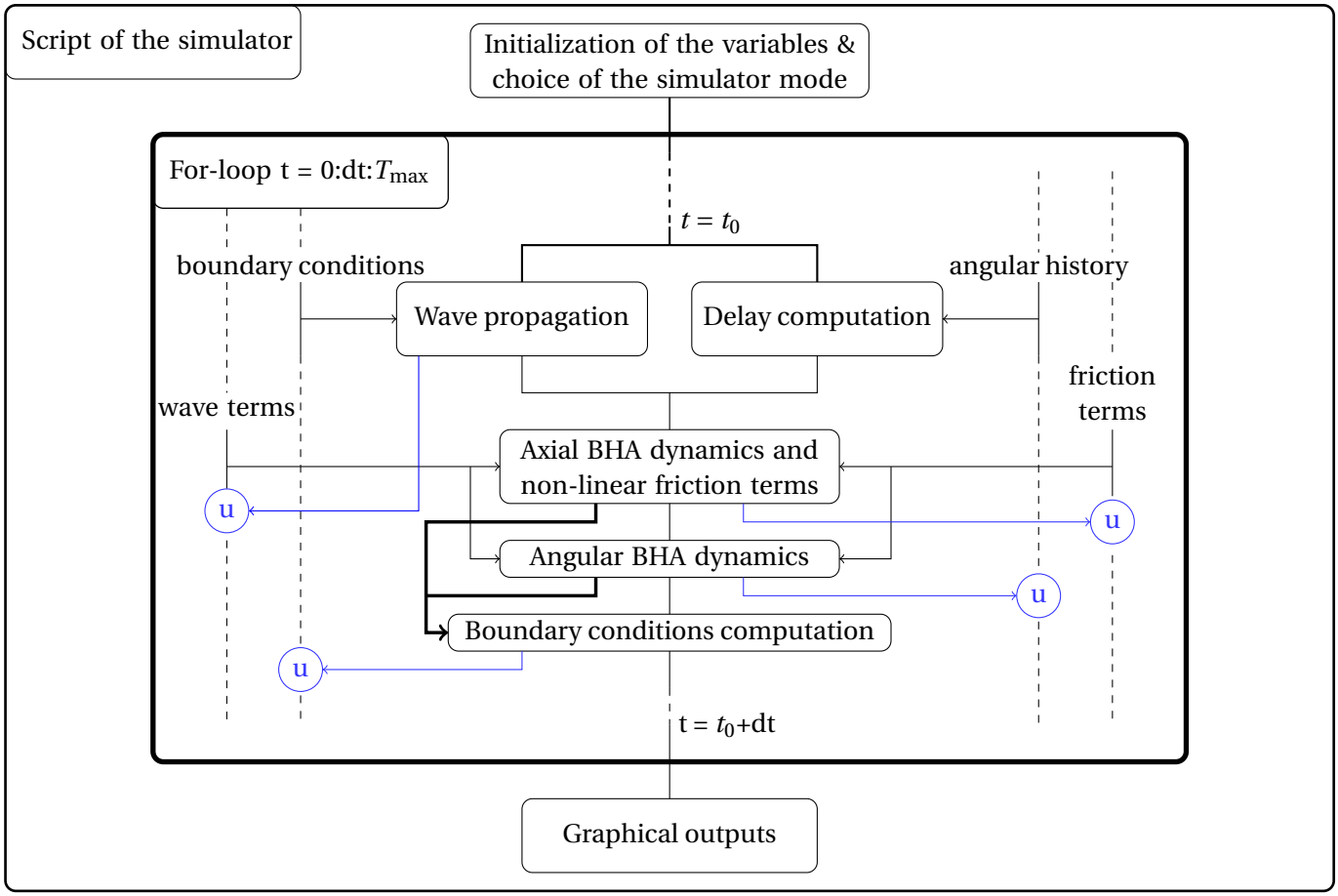

Figure II.1: *Flowchart representing the structure of the simulator*

The conventions used in this flowchart are explained in the following notes :

- The bold wide rectangle represents the integration loop of the simulator. It is used to compute the

solutions of the equations (I.24) over a given time period $[0, T_{\max}]$ with prescribed initial conditions using an Euler scheme.

- The smaller rectangular boxes represent the main actions performed by the script at each step of the loop in chronological order from top to bottom.

- The incoming arrows on the sides of the boxes account for the variables needed as inputs for the computations involved in this particular part of the code.

- The vertical dashed lines represent numerical quantities that are conserved during the whole simulation and that are needed for the next steps of the loop.

- The blue arrows terminated by a circled u stand for the *update* of the corresponding quantities.

Let us now describe more in details the different parts of the code illustrated in the flowchart II.1.

II.1.1 Main script of the simulator

The main script of the simulator is split into the three main parts highlighted in the flowchart II.1 : a definition of the solving mode and of the simulation parameters, the dynamics integration loop, and the generation of graphical outputs.

The definition of all the simulation parameters such as the physical constants of the system, the constants of the dynamics (I.24), the nondimensionalizing parameters, etc... is made in a side-script called at the beginning of each execution of the code. Let it be noted that this has no incidence in terms of efficiency since this script defines only scalar and fixed-size vectorial constants.

The next part of the main script is dedicated to defining the numerical parameters of the simulator, such as the size of the time and space steps for the integration procedures, the computation time $T_{\max}$ - noted `ind_max` when when discretized - , etc... as well as the different state variables of the system.

The presence of the delays in the dynamics calls for a constant need to have access to a varying number of past values of the state variable. To deal with this peculiarity as efficiently as possible, the choice was made to define an additional duration $D_{\max}$- similarly called `D_max` - corresponding to the maximal value authorized for the delays in the solving procedure. All the state variables of the problem are then stored in arrays of length `ind_max+D_max` so that the potentially required history of each state variable is available at each steps of the procedure, including the first one. This is illustrated in the figure II.2.

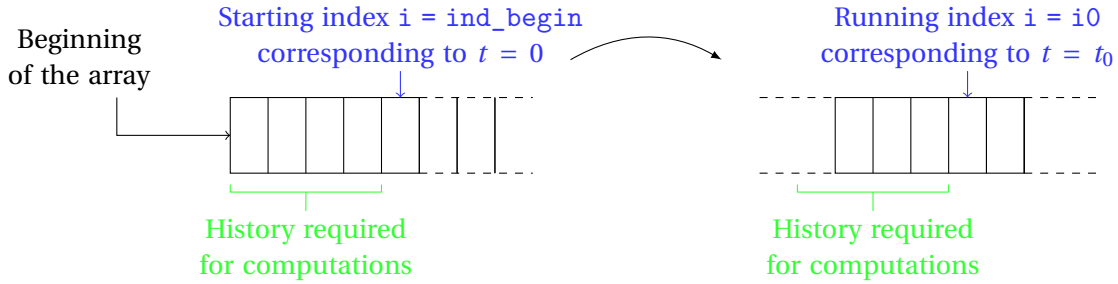

Figure II.2: *Illustration of the array structure used for the state variables*

This idea presents the nice features of increasing the size of the corresponding arrays only by a relatively small constant number of indices while enabling to implement the dynamics-related computation in a fashion very similar to the analytical expressions. For instance, one can transcript $z(\tau - \bar{\tau}_N - \tilde{\tau}_N)$ into `BHA_axial_velocity(i-tauN_ind-tauN_tilde_ind)` in keeping with the notations of the Matlab code. Moreover, it allows to manipulate fixed size arrays - Matlab may be rather bad performance-wise at handling size-varying arrays - without worrying about the running index being out of bounds.

Afterwards, the main script computes the numerical solution of (I.24) before plotting graphical outputs.

II.1.2 Dynamics integration loop

Let us now describe in ample detail the different parts of the integration loop sketched in figure II.1.

Wave propagation

The one time-step ahead wave propagation occurring in the drillpipes and satisfying the hyperbolic equations of (I.24) along with their boundary conditions was handled by using a solver coded by Florent Di Meglio. This solver is an explicit finite difference scheme for solving hyperbolic problems. It roughly is the analogous of a fourth order Runge-Kutta (hereafter referred to as RK4) procedure transposed in a hyperbolic PDE framework. I had to perform some minor modifications to insert it in the framework of the simulator, but nothing significant.

It has to be noted that the integration loop was designed so that the hyperbolic PDEs and the ODEs can be integrated simultaneously and cascaded into one another at each step of the loop. Thus, the time steps used for both dynamics are the same and their constant size $\mathrm{d}\tau$ is given here indirectly through

$$\mathrm{d}\tau = \frac{\mathrm{d}\chi}{\mathrm{CFL} \times \lambda_{\max}} \tag{II.1}$$

where $\mathrm{d}\chi$ is the space step fixed for the hyperbolic scheme, $\lambda_{\max}$ is the largest normalized propagation velocity involved in the hyperbolic equations and CFL is the Courant-Friedrichs-Lewy constant chosen for the system. This constant has to be larger or equal to 1, and in practice we always take CFL = 1 to limit numerical diffusion.

Computation of the delay

The computation of the time-varying delay $\tilde{\tau}_N(\cdot)$ is made by solving the implicit equation in $\tilde{\tau}_N$

$$\int_{\tau-\bar{\tau}_N-\tilde{\tau}_N}^{\tau} \omega(s)\mathrm{d}s + \omega_0\tilde{\tau}_N = 0 \tag{II.2}$$

This part proved to be rather costly at first in terms of computations. What is determined in practice is the index `tauN_ind+tauN_tilde_ind` of the total delay $\bar{\tau}_N + \tilde{\tau}_N$ such that the left part of (II.2) vanishes. To do so, one evaluates this term for delay indices `tauN_ind+tauN_tilde_ind` going from 0 to `D_max` using a for-loop structure which has a breaking condition when said term switches sign. Indeed, empirically, this term increases with $\bar{\tau}_N + \tilde{\tau}_N$ and crosses zero only once. It is thus not required to evaluate the left part of (II.2) for all the delay indices in `[0,D_max]`.

Adding this breaking condition prooved very efficient once we introduced the controls in our simulator since the total delays tend to be relatively small when the variations of the angular velocity $\omega(\cdot)$ are monitored. However, this computation does not seem likely to be performed without involving any loops, which makes it possibly costly even upon adding this breaking condition. A good improvement suggestion made by Marc Bonnet would be to procede by dichotomy instead of travelling along the whole interval `[0,D_max]`.

Axial and angular dynamics of the BHA

The axial and angular dynamics of the BHA are updated at each step of the loop using an Euler integration scheme. The main reasons for using this simple scheme - and not something more accurate such as a RK4 procedure - are the following :

- An Euler scheme calls for only one evaluation of the dynamics-function and thus only one computation of the delay. As we have seen in paragraph II.1.2 , computing the delay $\bar{\tau}_N + \tilde{\tau}_N(\cdot)$ at a given time is a costly operation. Hence, implementing a more precise procedure involving more than one computation of the delay would prove very inefficient computation-wise.

- Most of the schemes involving more than a single function evaluation at the running simulation time require evaluations at times which are not integer multiples of the simulation time step. This in practice is rather inconvenient when computing the associated delay with the method we exposed before. Indeed, which would be more suited between $\tilde{\tau}_N(\tau)$ and $\tilde{\tau}_N(\tau + \mathrm{d}\tau)$ to account for $\tilde{\tau}_N(\tau + \frac{1}{2}\mathrm{d}\tau)$ which in practice is no accessible to computation?

- As mentioned before, the size of the time step $d\tau$ used in this integration procedure is dictated by the size of the space step $d\chi$ along with the CFL constant of the system and the maximal propagation speed λ_{max} involved in the hyperbolic PDEs. In practice, the propagation speeds involved in oil-drilling systems are rather high, our time steps are thus bound to be rather small. Even upon taking CFL= 1, one has $d\tau \lesssim 5\times$1e-4 for $d\chi \simeq$ 1e-2.

The only remaining particularity here is the computation of the non-linear friction terms $g[\bullet]$. Let us recall here that this term is of paramount importance in the sense that it is the one inducing and "monitoring" the axial stick-slip phenomenon arising in the system. Finding in the litterature a precise description of how this term was to be implemented proved rather tough, so I came up with a personal technique inspired by the ideas of [1]. The implementation we made can be summed up simply through the following algorithm :

Algorithm 1 Algorithm used to compute $\big(z(\tau+d\tau), g[z(\tau+d\tau)]\big)$ using $\big(z(\tau), g[z(\tau)]\big)$ at each loop turn

$\big(z(\cdot), g[z(\cdot)]\big)$ *are known at time* τ *from the previous loop turn*

if $z(\tau) > -v_0$ **then** the system is in a slip phase

  $z(\tau+d\tau)$ *is computed using the Euler scheme*

  if $z(\tau+d\tau) > -v_0$ **then** the system remains in the slip phase
    $g[z(\tau+d\tau)] = 0$
  else if $z(\tau+d\tau) \leq -v_0$ **then** the system enters a stick phase
    $g[z(\tau+d\tau)] = \tilde{g}(\tau+d\tau)$
    $z(\tau+d\tau) = -v_0$
  end

else if $z(\tau) \leq -v_0$ **then** the system is in a stick phase

  $g[z(\tau+d\tau)] = \tilde{g}(\tau+d\tau)$

  if $g[z(\tau+d\tau)]S > 0$ **then** the system remains in the stick phase
    $z(\tau+d\tau) = -v_0$
  else if $g[z(\tau+d\tau)] \leq 0$ **then** the system enters a slip phase
    $z(\tau+d\tau)$ *is computed using the Euler scheme*
    $g[z(\tau+d\tau)] = 0$
  end

end

[1]

Here, $\tilde{g}(\cdot)$ is the same as defined in section I.4 and stands for the friction function $g[z(\cdot)]$ cancelling the axial dynamics.

Recall that $z(\cdot)$ is the non-dimensional velocity-perturbation around the non-dimensional equilibrium v_0 and that the stick-slip phenomenon depends on whether the total velocity $v(\cdot) = v_0 + z(\cdot)$ vanishes or not. This justifies our comparison choices in the previous algorithm [1].

The angular velocity $\omega(\cdot)$ is then computed at each step using the Euler scheme [2].

Boundary conditions

The last part of the integration loop is to update the boundary conditions of the hyperbolic equations system. One needs to update the $(\tilde{u}, \tilde{\phi})$ terms at $\chi = 0$ and $(\tilde{v}, \tilde{\psi})$ at $\chi = 1$ using the following principles

[1] In the code, all inequalities are to be satisfied within a tolerance ϵ which is fixed depending on the time-step precision.

[2] We recall that it would be possible to introduce an angular equivalent to our function $g[\bullet]$ but that it is not relevant for our purpose since we wish to stabilize the torsional dynamics around its equilibrium ω_0 and not to study a torsional stick-slip.

- The type of boundary conditions imposed at $\chi = 0$ can be chosen freely by the user - imposing velocity, torque, even taking into account an actuator dynamics - as described in the paragraph I.2.1. The wave-reflection part is not complicated, yet updating these boundary conditions gets difficult upon introducing the controller involving the prediction given by (IV.14). This part of the code is by far the costliest in terms of computation since it involves two nested for-loops that cannot be vectorized using higher dimension arrays.

- The boundary conditions imposed at $\chi = 1$ are velocity equilibriums between the drillpipes and the BHA. They can implemented straightforwardly using the corresponding equations given in (I.24).

II.1.3 Graphical outputs

Let us shortly describe the graphical outputs of the simulator. Recall that the main interest for us is to stabilize the ODE part of the dynamics (I.24), or namely to control the dynamics of the BHA. That is why the plots of biggest interest for us are those of the BHA axial and angular velocity. We will see later on that some other quantities may prove useful to look at, such as the modulus of their Fourier transform in order to perform spectral analysis, the delay $\bar{\tau}_N + \tilde{\tau}_N(\cdot)$ or the control $U(\cdot)$. All these quantities are displayed using simple Matlab plotting commands.

II.2 Open-loop simulations and frequency analysis of the BHA

Throughout Section II.1 was detailed the structure of the simulator that we implemented during this internship. In Subsections II.2.1 and II.2.2, we check its correctness by comparing our simulation results with those presented in [1], and also try and put to light relevant information for the oncoming control design.

II.2.1 Frequency analysis and comparison with the results of [1]

One of the first goals of my internship was to compare our results to those displayed in [1] even though the two approaches are rather different [3]. We thought that finding results being coherent with those of an article dedicated to the simulation of oil-drilling tool would be a good indicator of the liability of our simulator.

We found overall behaviour that were very similar to those of [1] (see figures II.5 and II.6), even though the presence of damping in their model induced some discrepancies, especially in terms of characteristic evolution times of the system. We then chose to make a comparison of our results in terms of *frequency analysis*, which might be less sensitive to small differences between models.

The figures II.3 and II.3 both represent the modulus of the Fourier transform of the axial and angular velocity of the BHA. Surprisingly enough, we obtained results very similar to those displayed in [1] for the angular velocity modes of oscillations and completely different ones for the axial velocity. More precisely :

- The remarkable frequencies expected for the axial dynamics in [1] are 1.63Hz, 3.91Hz and 6.41Hz while ours are 0.45Hz, 3.9Hz and 5.8Hz for the mild ones and 4.32Hz, 4.76Hz and 5.22Hz for the more pronounced ones as illustrated in figure II.3.

- On the other hand, the expected angular frequencies are 0.45Hz, 1.70Hz, 3.19Hz, 4.80Hz while we obtained 0.45Hz, 1.71Hz, 3.19Hz and 4.7Hz as illustrated in II.4.

The reason for the discrepancies related to the axial behaviour are yet unknown to us. However, both the similarities in terms of angular oscillations as well as the overall behaviours tend to confirm that our simulator is at the very least qualitatively sound and fairly accurate quantitatively speaking.

[3] They chose a distributed BHA model and implemented their solver using a finite element method. They also added some damping to the dynamics

Figure II.3: *Spectral analysis of the axial velocity of the BHA in the framework of our lump mass model*

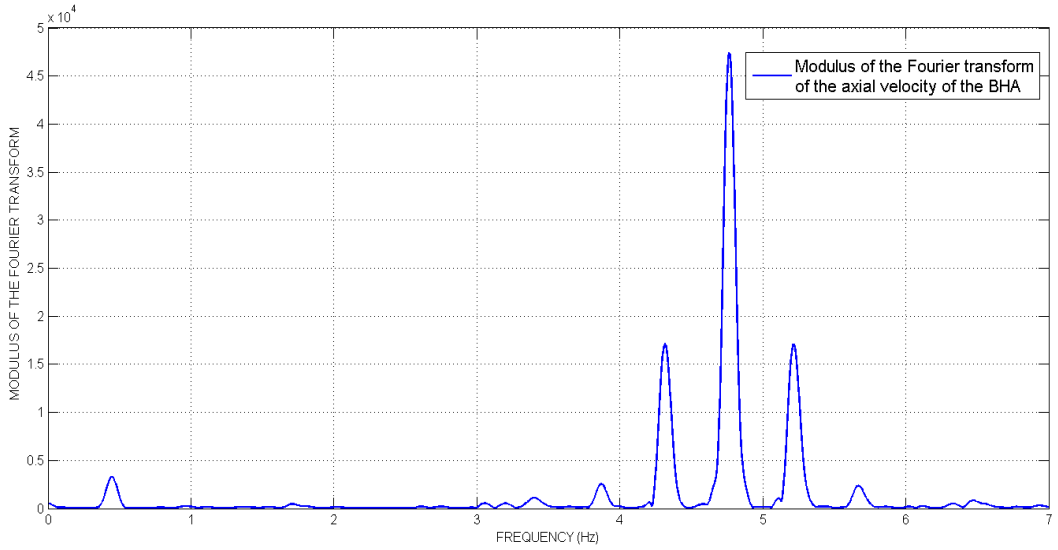

Figure II.4: *Spectral analysis of the angular velocity of the BHA in the framework of our lump mass model*

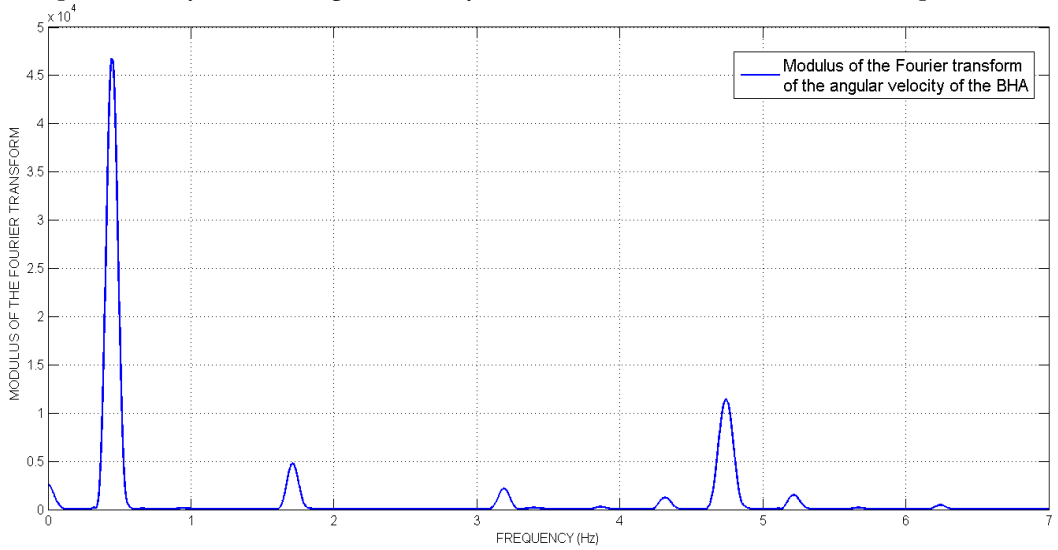

II.2.2 Open-loop simulations and overall behaviour

Let us now focus on the information the open-loop simulations can provide us with on the behaviour of the system.

The global behaviour of the angular velocity is mainly dictated by the nature of the boundary conditions imposed at $\chi = 0$ and by the magnitude of the initial angular perturbation relative to the axial one. We shall see that the trends are not quite similar depending on whether the user applies velocity conditions or torque conditions for the angular dynamics of the drillpipes. The axial overall behaviour on the other hand remains fairly invariant with any kind of initial condition. Contrary to the angular dynamics, there is no flexibility in the choice of the axial boundary conditions (see paragraph I.2.1).

Let us for instance have a look at the axial and angular velocity of the BHA stemming from an open-loop simulation with $T_{\max} = 7s$, where the initial conditions are given in the form of perturbations of both the BHA axial and angular velocity around their nominal values - with a perturbation 10 times bigger for the angular velocity - , and where we take a boundary condition of the form (I.4) at $\chi = 0$. This boundary condition corresponds to an arbitrarily fast actuator monitoring the angular velocity of the system. The axial and angular velocity of the BHA are respectively represented in the figures II.5 and II.6.

Some remarks can already be made based on these plots :

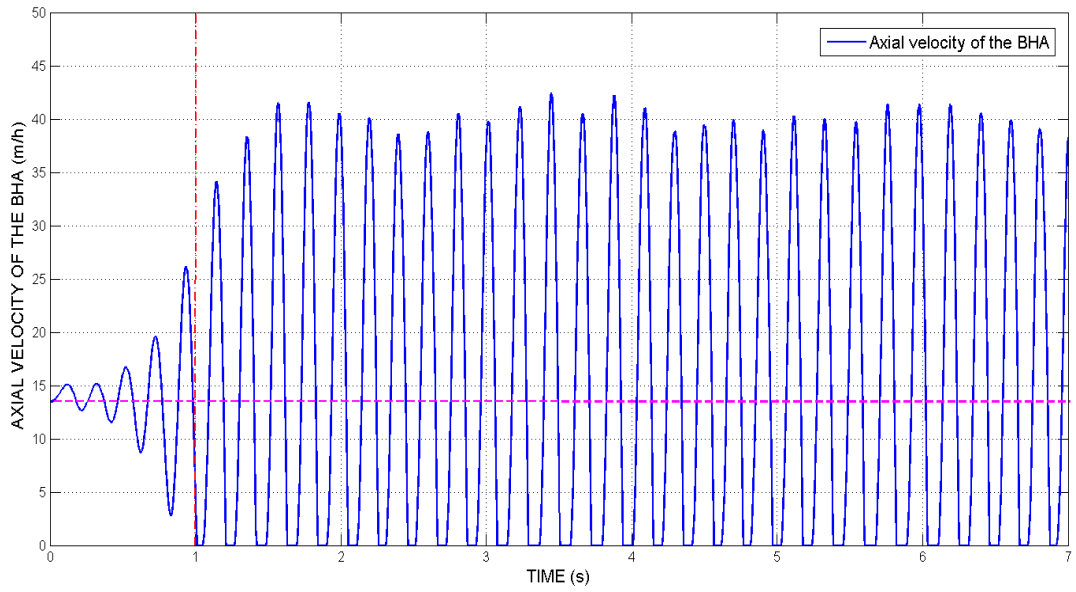

Figure II.5: *Axial velocity of the BHA with pure angular velocity conditions prescribed at $\chi = 0$. The red line marks the time at which the system enters its limit cycle and the pink one indicates the nominal axial velocity v_0*

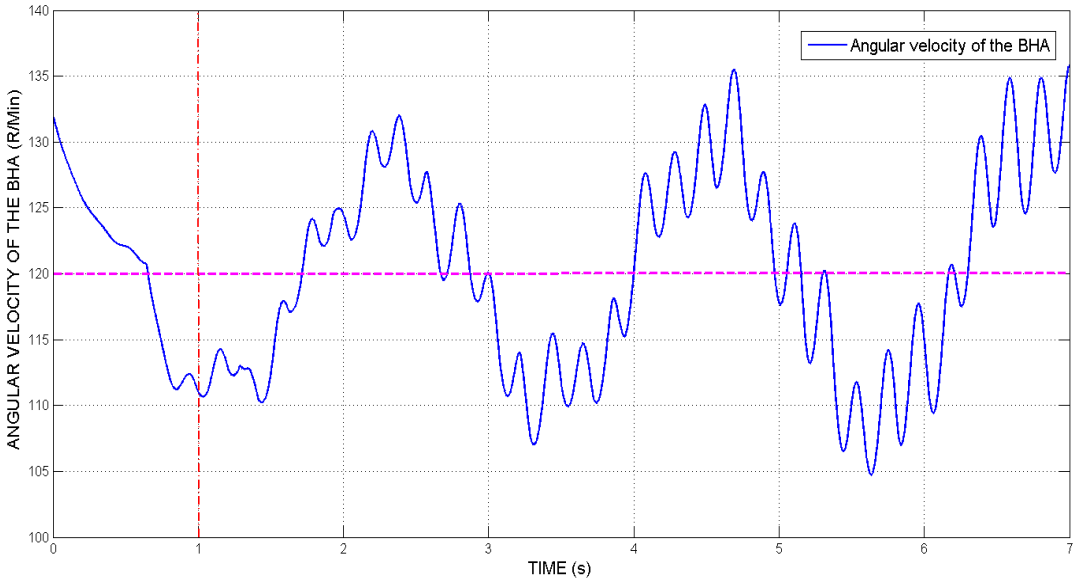

Figure II.6: *Angular velocity of the BHA with pure angular velocity conditions prescribed at $\chi = 0$. The red line marks the time at which the system enters its limit cycle and the pink one indicates the nominal angular velocity ω_0*

- One can clearly observe on figure II.5 the axial limit cycle which is reached by the system at time $t = 1s$. This constitutes one of the main discrepancy between our observations and the ones made in [1]. Indeed, in the simulation results of [1], the axial limit cycle is reached by the system for $t \gtrsim 40s$. This may be due to the presence of damping in their model which we did not consider in ours.

- As mentioned in the introduction, one can see here that the angular velocity, even though disturbed by fast oscillations induced by the axial dynamics, has oscillations much slower than those of the axial velocity.

Upon doing some more simulations while alternatively cancelling some of the terms in the dynamics (I.24) - the results of which being omitted for brevity - , we made some rather intriguig additional discoveries concerning the influence of the different terms on the dynamics.

- The axial limit cycle seems to be highly independant from the rest of the dynamics. For instance, even by setting $\omega(\cdot)$ to be constantly equal to its nominal value, leading to delays always equal to $\bar{\tau}_N$, the

axial dynamics reached its limit cycle in roughly 1 second. Besides, it also does not depend on the type of angular boundary conditions imposed at $\chi = 0$.

- ◇ The term that is the more disruptive and that generates the wildest behaviour in the angular dynamics is the velocity input from the BHA $\tilde{\phi}(1,\cdot)$. This seemed rather strange at first, all the more considering that this term is also the one through which our prediction-based controller - which we shall describe in section IV.3 - acts on the system. Yet, upon looking at the boundary conditions in (I.24), one can see that the waves modelled by the hyperbolic equations are reflected without loss at $\chi = 0$ and $\chi = 1$. Hence, the term $\tilde{\phi}(1,\cdot)$ at a time τ_0 accounts roughly for something of the form $\omega(\tau_0 - 2D_2)$ where $D_2 = \frac{L_*}{t_* c_\phi}$. The influence of this particular effect will be detailed in section IV.3 dedicated to the practical implementation of the controller and simulation results.

As displayed through the previous enumerations, we were able using simulation results to obtain some insightful information on the dynamics of our system. However, carrying out an adapted controller synthesis calls for precise and analytical results concerning the qualitative behaviour we highlighted. The coming chapter is hence dedicated to the second main contribution of this work : the semi-analytical analysis of the axial limit cycle.

Part III

Mathematical analysis of the axial limit cycle of the lump BHA

As it was already mentioned earlier in this report, the pseudo-period of the axial limit cycle is too small for an actuator to try and control it. Similarly, the axial terms involved in the angular dynamics will not be accessible to exact compensations by a controller. However, it occured to us that a deeper understanding of this cycle could prove useful in terms of control design.

The following development constitues one of the main contributions of my internship. Based on existing articles - [5] to quote one - we adapted a semi-analytical method to studying stick-slip cycles to our BHA model in order to refine our control design (described in section IV.3).

III.1 Complete analysis of the limit cycle and its governing equations

In the framework of this analysis, we will only consider the axial dynamics of the system. Moreover we will make the following assumptions :

- The velocity input of the drillpipes $\tilde{u}(1,\cdot)$ is constant over one stick-slip cycle.
- The variations of the error delay of the system $\tilde{\tau}_N(\cdot)$ are commensurate to the those of the angular velocity $\omega(\cdot)$ through equation (II.2). Given the facts that the axial limit cycle has a period much smaller than the angular dynamics and that its influence on said dynamics is mild, it is not unrealistic to assume that the error delay $\tilde{\tau}_N(\cdot)$ is constant over one stick-slip cycle.

We shall henceforth note $\tilde{u}(1,\cdot) := u$ and $\bar{\tau}_N + \tilde{\tau}_N := \tau_N$, both begin constants.
The dynamics of the axial limit cycle obeys the equations

$$\begin{cases} \dot{x}(\tau) = z(\tau) \\ \dot{z}(\tau) = c_0^z\,[u - z(\tau)] - c_1\,[x(\tau) - x(\tau - \bar{\tau}_N - \tilde{\tau}_N)] - c_2\tilde{\tau}_N + \lambda c_1 g[z(\tau)] \end{cases} \tag{III.1}$$

in keeping with the notations introduced in (I.24) and introducing the variable $x(\cdot)$ - the axial position - which derivative is the axial velocity $z(\cdot)$.

In what follows, it will be more convenient to work with the following centered variables :

$$x(\tau) \equiv x(\tau) + v_0\tau \quad , \quad z(\tau) \equiv z(\tau) + v_0 \tag{III.2}$$

The dynamics (III.1) thus takes the form

$$\begin{cases} \dot{x}(\tau) = z(\tau) \\ \dot{z}(\tau) = -c_0^z z(\tau) - c_1\,[x(\tau) - x(\tau - \bar{\tau}_N - \tilde{\tau}_N)] + \lambda c_1 g(z) + \gamma \end{cases} \tag{III.3}$$

where $\gamma = c_0^z(u + v_0)$ is a constant.

In the framework of the model we chose - to a great extent inspired by [5] - , the properties of the stick-slip cycle will be entirely determined by the three following constant parameters :

- The time τ_b defined such that the duration of the stick-slip cycle be equal to $\tau_N + \tau_b$.

- The time τ_a defined such that the duration of the slip phase of the cycle is equal to $\tau_a + \tau_b$.

- The axial jump x_{lim} corresponding to the difference between two successive values of the axial position x of the system during the stick-phase.

Figure III.1 shows a detailed version of one stick-slip cycle [1]. Using the definition of the constants τ_a, τ_b and x_{lim}, it can be split into the following phases :

◇ Phase a ($0 \leq \tau \leq \tau_a$) : The system is in a slip-phase, hence $g = 0$ in (III.3). Here the delayed term $x(\cdot - \tau_N)$ is non-zero and has the same form as the non-delayed solution $x(\cdot)$ in phase b but with different boundary conditions.

◇ Phase b ($\tau_a \leq \tau \leq \tau_a + \tau_b$) : The system is in a slip-phase and both g and $x(\cdot - \tau_N)$ are equal to 0.

◇ Phase c ($\tau_a + \tau_b \leq \tau \leq \tau_N$) : The system is in the part of the stick-phase where the delayed term $x(\cdot - \tau_N)$ is constant and equal to 0.

◇ Phase d and e ($\tau_N \leq \tau \leq \tau_N + \tau_b$) : The system is in the part of the stick-phase where $x(\cdot - \tau_N) \neq 0$. Phase d corresponds to $\tau_N \leq \tau \leq \tau_N + \tau_a$ where the solution of phase a is used to compute $x(\cdot - \tau_N)$ and phase e to $\tau_N + \tau_a \leq \tau \leq \tau_N + \tau_b$ where the solution of the phase b is used to compute $x(\cdot - \tau_N)$.

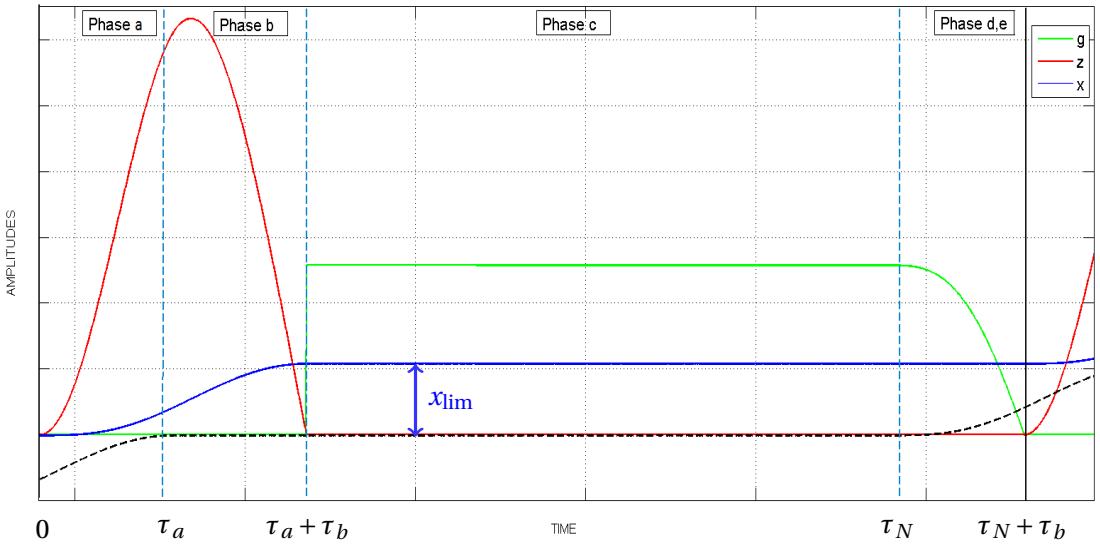

Figure III.1: *Zoomed-in representation of one stick-slip cycle of the axial dynamics of the BHA with the axial position $x(\cdot)$ (blue), the axial velocity $z(\cdot)$ (red), the non-linear friction function $g[z(\cdot)]$ (green) and the delayed position $x(\cdot - \tau_N)$ (dashed black)*

The goal of our semi-analytical approach was to derive closed-form equations satisfied by the three parameters τ_a, τ_b and x_{lim}. We obtained the equations (III.5) using the following junctions conditions :

$$x_a(\tau_a) = x_b(\tau_a) \ , \ x_b(\tau_a + \tau_b) = x_{\text{lim}} \ , \ \tilde{g}(\tau_N + \tau_b) = 0 \tag{III.4}$$

where $x_a(\cdot) = x|_{[0,\tau_a]}(\cdot)$, $x_b(\cdot) = x|_{[\tau_a, \tau_a+\tau_b]}(\cdot)$ and $\tilde{g}(\cdot)$ is the same as defined in (I.24).

Doing so required a fairly good amount of algebra, for which details are given in appendix A, and led to the following set of equations satisfied by τ_a, τ_b and x_{lim} :

[1] It is assumed here for simplicity that the cycle starts at $\tau = 0$ and that $x(0) = 0$

$$x_{\lim} = \begin{cases} \dfrac{\gamma}{c_1}\left(\dfrac{2-e^{\frac{c_0^z}{2}\tau_a}\left[\cos\left(\frac{1}{2}\sqrt{\Delta}\tau_a\right)+\frac{c_0^z}{\sqrt{\Delta}}\sin\left(\frac{1}{2}\sqrt{\Delta}\tau_a\right)\right]}{1-e^{\frac{c_0^z}{2}\tau_a}\left[\cos\left(\frac{1}{2}\sqrt{\Delta}\tau_a\right)+\frac{c_0^z}{\sqrt{\Delta}}\sin\left(\frac{1}{2}\sqrt{\Delta}\tau_a\right)\right]}\right) & \text{if } \tau_b \geq \tau_a \quad (\text{namely } x_{\lim} = \dfrac{\gamma}{c_1} + x_b(\tau_b) \\ \dfrac{\gamma}{c_1} + x_a(\tau_b) & \text{if } \tau_b \leq \tau_a \quad (\text{too long to be detailed}) \end{cases}$$

$$\frac{\gamma}{c_1} + \left(x_{\lim} - \frac{\gamma}{c_1}\right) e^{\frac{c_0^z}{2}\tau_b}\left[\cos\left(\frac{1}{2}\sqrt{\Delta}\tau_b\right) - \frac{c_0^z}{\sqrt{\Delta}}\sin\left(\frac{1}{2}\sqrt{\Delta}\tau_b\right)\right] = \left(2\frac{\gamma}{c_1} - x_{\lim}\right) \times \left(1 - e^{-\frac{c_0^z}{2}\tau_a}\left[\cos\left(\frac{1}{2}\sqrt{\Delta}\tau_a\right) + \frac{c_0^z}{\sqrt{\Delta}}\sin\left(\frac{1}{2}\sqrt{\Delta}\tau_a\right)\right]\right) + \left(\frac{\gamma}{c_1} - x_{\lim}\right) \times \left(\frac{c_0^z c_1 \tau_a}{\Delta} - \frac{2c_1}{\Delta}\left[\sin\left(\frac{1}{2}\sqrt{\Delta}\tau_a\right)^2 + \frac{c_0^z}{2\sqrt{\Delta}}\sin\left(\sqrt{\Delta}\tau_a\right)\right]\right)$$

$$2\left(x_{\lim} - \frac{\gamma}{c_1}\right) e^{\frac{c_0^z}{2}\tau_b}\sin\left(\frac{1}{2}\sqrt{\Delta}\tau_b\right) + 2\left(2\frac{\gamma}{c_1} - x_{\lim}\right) e^{-\frac{c_0^z}{2}\tau_a}\sin\left(\frac{1}{2}\sqrt{\Delta}\tau_a\right) = \left(\frac{\gamma}{c_1} + x_{\lim}\right)\frac{(2c_1\tau_a - c_0^z)}{\Delta} + \left(\frac{\gamma}{c_1} - x_{\lim}\right) \times \left[\sin\left(\frac{1}{2}\sqrt{\Delta}\tau_a\right) + \frac{c_0^z}{\sqrt{\Delta}}\cos\left(\frac{1}{2}\sqrt{\Delta}\tau_a\right)\right]\left[\cos\left(\frac{1}{2}\sqrt{\Delta}\tau_a\right) - \frac{c_0^z}{\sqrt{\Delta}}\sin\left(\frac{1}{2}\sqrt{\Delta}\tau_a\right)\right] \quad \text{(III.5)}$$

where $\Delta = 4c_1 - (c_0^z)^2 > 0$ since $c_0^z \simeq 12.5$ and $c_1 \simeq 3 \times 1e3$.

From the first equation of (III.5), one has that $x_{\lim}$ is proportional to γ [2]. Since all the terms in the second and third equations of (III.5) are proportional to linear combinations of $x_{\lim}$ and γ, all the γ terms factorize and drop, leaving these two equations characterizing τ_a and τ_b independant from γ and thus from u. This leads to the following theorem which sums up our results and observations concerning the axial limit cycle.

Theorem 1. *The three parameters τ_a, τ_b and x_{lim} introduced in the framework of the stick-slip model inspired from [5] fully describe the behaviour of the axial stick-slip cycle governed by the equations* (III.3)*. Moreover, the two time constants τ_a and τ_b depend **only** on the physical parameters of the system through the constants c_0^z, c_1 and c_2 defined in section I.4.*

This independence result is extensively interesting for the following reasons :

- ◇ The model proposed in [5] that we transposed here implies that the three constants τ_a, τ_b and $x_{\lim}$ be independent from the delay τ_N of the system [3]. However, they could still have involved the velocity input from the drillpipes u, which we assumed here to be constant over a stick-slip cycle for simplicity, but which is not in practice. A dependence of this type for τ_a and τ_b - which would probably have been very implicit - would have made it impossible to perform a time averaging of the stick-slip cycle.
- ◇ This result corroborates our observation of section II.2.2 that the time-related behaviour of the axial limit cycle seemed rather independent from the initial conditions of the system, the angular dynamics, the fact that we cancel or not some of the terms involved in the dynamics, etc...

The last step of this semi-analytical study was the numerical computation of the constants τ_a, τ_b and $x_{\lim}$. We represent in Table III.1 some simulation results that aim at both computing the three constants and studying empirically their independence from τ_N and u.

[2] The explicit expression for $x_a(\cdot)$ displayed in A shows that it is proportional to γ.

[3] For which the assumption of being constant during one stick-slip cycle is rather accurate.

$\frac{u}{v_0}$	$\frac{\tau_N}{\bar{\tau}_N/t_*}$	$(\tau_a^{\text{sim}}, \tau_a^{\text{ana}})$	$\delta\tau_a$	$(\tau_b^{\text{sim}}, \tau_b^{\text{ana}})$	$\delta\tau_b$	$(x_{\text{lim}}^{\text{sim}}, x_{\text{lim}}^{\text{ana}})$	δx_{lim}
6	6	(3.57,3.58)× 1e-2	4.02 × 1e-3	(3.57,3.53)× 1e-2	1.05 × 1e-2	(4.16,4.24)× 1e-1	1.87 × 1e-2
6	4	(3.56,3.58)× 1e-2	4.47 × 1e-3	(3.56,3.53)× 1e-2	7.38 × 1e-3	(4.19,4.24)× 1e-1	1.22 × 1e-2
6	0.8	(4.18,3.58)× 1e-2	1.66 × 1e-1	(3.67,3.53)× 1e-2	3.95 × 1e-2	(4.34,4.24)× 1e-1	2.45 × 1e-2
2	6	(3.56,3.58)× 1e-2	6.23× 1e-3	(3.56,3.53)× 1e-2	6.69 × 1e-3	(3.39,3.43)× 1e-2	9.94 × 1e-3
2	4	(3.56,3.58)× 1e-2	6.02× 1e-3	(3.55,3.53)× 1e-2	5.03 × 1e-3	(4.18,3.43)× 1e-2	6.17 × 1e-3
2	0.8	(3.67,3.58)× 1e-2	1.66 × 1e-1	(3.56,3.53)× 1e-2	3.95 × 1e-2	(3.51,3.43)× 1e-2	2.43 × 1e-2

Table III.1: *Simulation results for the computations of $(\tau_a^{sim}, \tau_a^{ana})$, $(\tau_b^{sim}, \tau_b^{ana})$ and $(x_{lim}^{sim}, x_{lim}^{ana})$, along with their relative error $(\delta\tau_a, \delta\tau_b, \delta x_{\text{lim}})$ and different values for the u and τ_N*

We denote by $\bullet^{\text{ana}}$ the quantities computed using the analytical expressions (III.5) [4], by $\bullet^{\text{sim}}$ those computed empirically by measuring the length of the stick and slip phases observed from simulations of the system (III.3) and by $\delta\bullet$ the relative errors between the analytical and empirical quantities.

We obtain that the two analytical values for τ_a and τ_b are given by

$$\tau_a^{\text{ana}} = 3.58 \times \text{1e-2} \ , \ \tau_b^{\text{ana}} = 3.53 \times \text{1e-2} \tag{III.6}$$

Let us make some comments concerning the results displayed in Table III.1.

- ◇ One can see that even though (τ_a, τ_b) are assumed to be independent from u and τ_N, it is not completely true in practice. However empirically, upon controlling even approximately the torsional dynamics of the system, the total delay $\tau_N = \bar{\tau}_N + \tilde{\tau}_N$ remains within an interval of the form $[0.9\bar{\tau}_N, 2\bar{\tau}_N]$ and the velocity input u within an interval of the form $[-3v_0, 3v_0]$. As illustrated in Table III.1, these intervals correspond to a satisfactory validity of the model since the relative errors between analytical and empirical values of the variables are of order $\delta \lesssim 1\%$
- ◇ In the model introduced in [5] it is assumed that $\tau_a \leq \tau_b$. In our case, we obtained that $\tau_a \geq \tau_b$, and numerically solving equations (III.5) subject to the constraint $\tau_a \leq \tau_b$ we always obtained $\tau_a^{\text{ana}} = \tau_b^{\text{ana}}$. We thus wondered whether there could be a need to redefine the constants τ_a and τ_b in the sense that the largest of the two quantities be always corresponding to τ_b and the smallest to τ_a. This hypothesis was however disputed by computing $\| x^{\text{sim}} - x^{\text{ana}} \|_{L^2([0,\tau_N+\tau_b])} / \| x^{\text{sim}} \|_{L^2([0,\tau_N+\tau_b])}$ where $x^{\text{sim}}(\cdot)$ is the solution $x(\cdot)$ obtained through the simulation of (III.3) and $x^{\text{ana}}(\cdot)$ is computed using $(\tau_a^{\text{ana}}, \tau_b^{\text{ana}}, x_{\text{lim}}^{\text{ana}})$ with the analytical expressions displayed in appendix A and taking alternatively $\tau_a^{\text{ana}} \leq \tau_b^{\text{ana}}$ and $\tau_a^{\text{ana}} \geq \tau_b^{\text{ana}}$. The relative L^2-norm error was much larger in the first case than in the second where it was almost null, tending to confirm that even though our results do not satisfy the condition $\tau_a \leq \tau_b$ they are the most fitting to our case.

III.2 Time averaging of the axial stick-slip cycle

As mentioned previously on several occasions, the main reason motivating this cycle analysis is that the terms of the torsional dynamics involving axial contributions are too fast to be compensated by a reasonable actuator. However, upon doing a time averaging of the terms stemming from the axial limit cycle, one could hope to partly compensate the axial contributions disturbing the torsional dynamics.

Upon assuming that the axial limit cycle phenomenon is almost perfectly periodic and that each period is roughly described by the stick-slip cycle studied in Section III.1 [5], the time averaging of a given quantity $f(\cdot)$ reads

$$\langle f \rangle = \lim_{T\to\infty} \left[\frac{1}{T} \int_0^T f(s)\mathrm{d}s \right] = \frac{1}{\tau_N + \tau_b} \int_0^{\tau_N+\tau_b} f(s)\mathrm{d}s \tag{III.7}$$

where we recall that $\tau_N = \bar{\tau}_N + \tilde{\tau}_N$.

[4] In practice, we searched for the values of τ_a, τ_b and x_{lim} which minimized the square of the absolute value of equations (III.5)

[5] This assumption is conditional to the fact that the variations of u and τ_N have a minor impact on the stick-slip cycle and that they are roughly constant on each individual cycle.

The analytical expressions for $x(\cdot)$ and $g[z(\cdot)]$ are given in appendix A. However, computing averagings using them would prove too cumbersome analytically and impractical in our solver. Besides, our approach is already somewhat approximative here, making it rather unnecessary to do our numerical computations with a full analytical precision.

We thus chose to perform our averaging using the following piecewise linear approximations

$$x(\tau) - x(\tau - \bar{\tau}_N - \tilde{\tau}_N) = \begin{cases} \frac{x_{\lim}}{\tau_b}(\tau_a - \tau) & \forall \tau \in [0, \tau_a] \\ \frac{x_{\lim}}{\tau_b}(\tau - \tau_a) & \forall \tau \in [\tau_a, \tau_a + \tau_b] \\ x_{\lim} & \forall \tau \in [\tau_a + \tau_b, \bar{\tau}_N + \tilde{\tau}_N + \tau_a] \\ \frac{x_{\lim}}{\tau_b}(\tau_a - \tau) & \forall \tau \in [\bar{\tau}_N + \tilde{\tau}_N + \tau_a, \bar{\tau}_N + \tilde{\tau}_N + \tau_b] \end{cases} \tag{III.8}$$

and

$$g[z(\tau)] = \begin{cases} 0 & \forall \tau \in [0, \tau_a + \tau_b] \\ \frac{1}{\lambda}\left(x_{\lim} - \frac{\gamma^z}{c_1^z}\right) & \forall \tau \in [\tau_a + \tau_b, \bar{\tau}_N + \tilde{\tau}_N] \\ \frac{1}{\lambda}\left(x_{\lim} - \frac{\gamma^z}{c_1^z}\right)\frac{\bar{\tau}_N + \tilde{\tau}_N + \tau_b - \tau}{\tau_b} & \forall \tau \in [\bar{\tau}_N + \tilde{\tau}_N, \bar{\tau}_N + \tilde{\tau}_N + \tau_b] \end{cases} \tag{III.9}$$

The result of this approximate time averaging procedure is shown in Figure III.2.

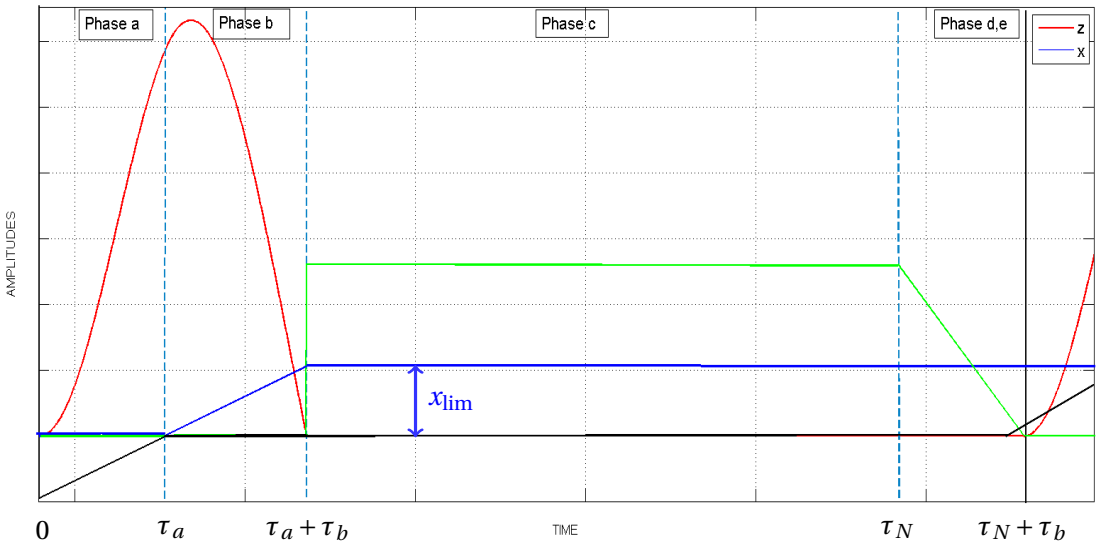

Figure III.2: *Representation of the piecewise linear approximations chosen for $x(\cdot)$ (blue), $g[z(\cdot)]$ (green) and the delayed position $x(\cdot - \tau_N)$ (black)*

These approximations yield the following averaged quantities

$$\begin{cases} \langle x(\cdot) - x(\cdot - \bar{\tau}_N - \tilde{\tau}_N) \rangle = \left(\frac{\bar{\tau}_N + \tilde{\tau}_N - \tau_a + \frac{\tau_b}{2} + \frac{\tau_a^2}{2\tau_b}}{\bar{\tau}_N + \tilde{\tau}_N + \tau_b} \right) x_{\lim} \\ \langle g[z(\cdot)] \rangle = \left(x_{\lim} - \frac{\gamma^z}{c_1^z} \right) \frac{\bar{\tau}_N + \tilde{\tau}_N - \tau_a - \frac{\tau_b}{2}}{\lambda(\bar{\tau}_N + \tilde{\tau}_N + \tau_b)} \end{cases} \tag{III.10}$$

However, having a non-linear expression of $\tilde{\tau}_N$ would prove rather inconvenient in terms of control considering that is in practice an integral term involving the angular velocity $\omega(\cdot)$. Thus, we linearized the expressions (III.10) with respect to $\tilde{\tau}_N$ - for convenience - under the assumption $\tilde{\tau}_N / (\bar{\tau}_N + \tau_b) \ll 1$ [6], leading to

[6] Assumption which is legit in practice upon controlling the torsional dynamics since $\tilde{\tau}_N$ is then close to 0.

$$\begin{cases} \langle x(\tau) - x(\tau - \bar{\tau}_N - \tilde{\tau}_N)\rangle = x_{\text{lim}} \left(\dfrac{\bar{\tau}_N - \tau_a + \frac{\tau_b}{2} + \frac{\tau_a^2}{2\tau_b}}{\bar{\tau}_N + \tau_b} \right) + x_{\text{lim}} \left(\dfrac{\tau_a + \frac{\tau_b}{2} - \frac{\tau_a^2}{2\tau_b}}{(\bar{\tau}_N + \tau_b)^2} \right) \tilde{\tau}_N + o(\tilde{\tau}_N) \\ \langle g[z(\tau)]\rangle = \left(x_{\text{lim}} - \dfrac{\gamma^z}{c_1^z} \right) \left(\dfrac{\bar{\tau}_N - \tau_a - \frac{\tau_b}{2}}{\lambda(\bar{\tau}_N + \tau_b)} \right) + \left(x_{\text{lim}} - \dfrac{\gamma^z}{c_1^z} \right) \left(\dfrac{\tau_a + \frac{3}{2}\tau_b}{(\bar{\tau}_N + \tau_b)^2} \right) \tilde{\tau}_N + o(\tilde{\tau}_N) \end{cases} \tag{III.11}$$

These averaged quantities will prove useful for designing a refined controller, as discussed in Section IV.3.

Part IV

Control of the dynamics of the BHA and introduction to the main tools of delayed-system control

Since the first papers (see for instance [6]) on the topic written by Smith in the 50's, delayed dynamical systems have been the interest of a (rather) small but very strong community of researchers due to their wide applications and mathematical peculiarities.

In many applications, the notion of delay - be it for the input of the system or for the state - appears quite naturally. One could for instance consider biological models such as prey-predators dynamics or engine motors models (see [7]). Moreover, delays are well known for any person studying dynamical systems to be one of the major causes of instability.

We will aim in the first place at presenting some mathematical results on which the theory of delayed-systems is based and then detail their recent extensions to more complicated systems encompassing the dynamics (I.24) that we study in this work.

IV.1 General introduction to the stabilization of delayed-dynamical systems

IV.1.1 Historical control design for a linear input-delay system : the Smith predictor

Let us consider the general case of a linear input-delayed dynamical system

$$\forall\, t \in \mathbb{R}_+ \ , \ \dot{X}(t) = AX(t) + BU(t-D) \tag{IV.1}$$

where $X(\cdot) \in \mathbb{R}^n$, $U(\cdot) \in \mathbb{R}^m$, $A \in M_{n\times n}(\mathbb{R})$, $B \in M_{n\times m}(\mathbb{R})$ and $D \in \mathbb{R}_+$ is a constant delay.

For a classical non-delayed dynamical system, namely taking $D = 0$, one would design a controller of the form $U(\cdot) = KX(\cdot)$ where the gain K is taken such that the matrix $(A+BK)$ is Hurwitz to get exponential stability. Here however, applying brutally the same idea would not work for the case $D \neq 0$ since it would lead to an equation involving both $X(t)$ and $X(t-D)$.

The method initially introduced by Smith in [6] is referenced to as *Prediction-based controller design* in the litterature. The idea is the following, instead of defining the control $U(\cdot)$ as a pure feedback, consider

$$\forall\, t \in \mathbb{R}_+ \ , \ U(t) = KX(t+D) \tag{IV.2}$$

which accounts for a prediction of the state $X(\cdot)$ over a time period D. Since $X(\cdot)$ satisfies the dynamics (IV.1), one can write the variation of constant formula to get

$$\begin{aligned} X(t+D) &= e^{AD}X(t) + \int_t^{t+D} e^{A(t+D-s)}BU(s-D)\mathrm{d}s \\ &= e^{AD}X(t) + \int_{t-D}^{t} e^{A(t-s)}BU(s)\mathrm{d}s \end{aligned} \tag{IV.3}$$

by doing the change of variable $s \equiv s - D$.

Hence, it is then possible to implement the prediction-based controller since it only involves an integral over the past values of the control and the running value of the state. Let it be noted however that the control becomes an infinite dimensional object.

Remark. As noted in several papers in the litterature all cited in [**?**], the choice of the discretization scheme used to compute the intregral has an important role in the numerical behaviour of the system. It was for instance shown that using a standard quadrature rule scheme could lead to diverging controls for arbitrary small integration steps.

The merits of this type of controller can easily be checked on simple examples of linear input-delay systems of the form (IV.1).

Consider the following example

$$A = \begin{pmatrix} 0 & 1 \\ -2 & 0 \end{pmatrix} \ , \ B = \begin{pmatrix} 0 \\ 2 \end{pmatrix} \ , \ D = 0.4 \ , \ K = -2 \tag{IV.4}$$

Illustrated in figure and IV.1.

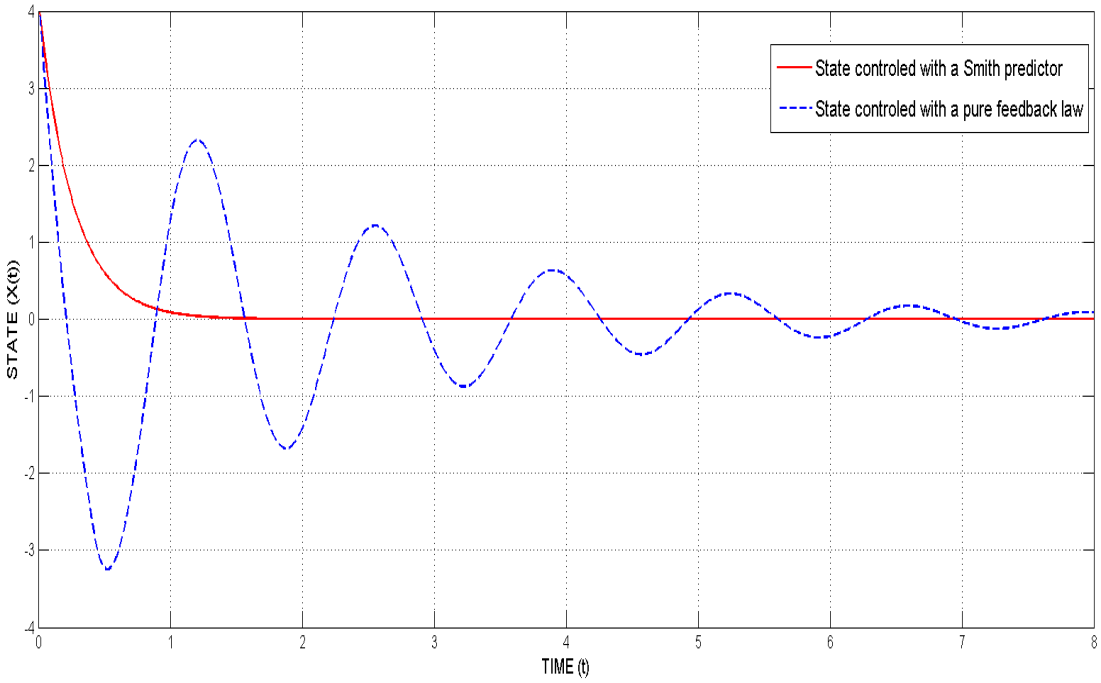

Figure IV.1: *Illustration of the merits of the prediction based controller (red) compared to a classical feedback (blue) on a delayed harmonic oscillator*

One can easily notice on these two examples that the Smith predictor is much more efficient performance-wise than a classical feedback approach to stabilize an linear input-delay system. Some small developments concerning the robustness of the predictor will be given in appendix B.

IV.1.2 A PDE inspired method : the backstepping approach

Short introduction to the main ideas of the PDE backstepping approach

Originally, this more recent formalism was introduced a decade ago by Krstic & Smyshlyaev (see for instance [8] and [9]) to study the stability of hyperbolic PDEs. It allows to ground the stability analysis of an hyperbolic PDE on classical (yet generalized) Lyapunov-Krasovskii arguments.

Remark. Let it be noted that the term *backstepping* does not directy relate to the classical term used to characterize the stabilization of cascaded ODE systems. It has been inspired by this classical approach in the sense that it can too be interpreted as a cascaded control-structure.

The main idea of this method is to find an invertible integral transformation depending on a given kernel that will map the original PDE system and its boundary conditions to a convenient target system which we know to be stable in some sense (exponentially, asymptotically, etc...). It has the nice feature to provide one with the explicit design of the corresponding control. Let us detail very briefly this notion on a simple example taken from Miroslav Krstic's book *Control of PDEs : A Course on Backstepping Design* [10], chapter 9.

Consider the following linear hyperbolic system

$$\forall (x,t) \in [0,1] \times \mathbb{R}_+ \ , \ \frac{\partial u}{\partial t}(x,t) - \frac{\partial^2 u}{\partial x^2}(x,t) = \lambda u(x,t) \ , \ \begin{cases} u(0,t) = 0 \\ u(1,t) = U(t) \end{cases} \tag{IV.5}$$

where $U(\cdot)$ is a control **which we aim at designing**. It can be shown that the open-loop system corresponding to (IV.5) is unstable with arbitrary many unstable eigenvalues depending on the value of the parameter λ (see [10]).

The idea here will be to introduce an infinite-dimensional change of coordinates in the form

$$\forall (x,t) \in [0,1] \times \mathbb{R}_+ \ , \ w(x,t) = u(x,t) - \int_0^x k(x,y)\,u(y,t)\mathrm{d}y \tag{IV.6}$$

mapping our system (IV.5) to the following exponentially stable target system

$$\forall (x,t) \in [0,1] \times \mathbb{R}_+ \ , \ \frac{\partial w}{\partial t}(x,t) - \frac{\partial^2 w}{\partial x^2}(x,t) = 0 \ , \ \begin{cases} w(0,t) = 0 \\ w(1,t) = 0 \end{cases} \tag{IV.7}$$

Other benefits of this kind of transformation are described in the following statements

- The condition $w(1,\cdot) = 0$ gives immediatly using (IV.6) the control law $U(\cdot) = \int_0^1 k(1,y)\,u(y,\cdot)\mathrm{d}y$ enabling to stabilize exponentially the original system (IV.5).
- The coordinate transformation displayed in (IV.6) is a Volterra integral transformation, which has the nice feature of always being invertible
- In the general case, the computation of the kernel $k(\cdot,\cdot)$ always follows the same idea. Imposing the form of the hyperbolic equation in (IV.7) leads to a PDE satisfied by $k(\cdot,\cdot)$. This approach can however be rather cumbersome even in simple cases.

Here, it is trivial that the target system is exponentially stable since it is a linear hyperbolic system with zero-boundary conditions and zero-source terms. However, in the general case, one will have to perform a Lyapynov analysis in the sens of some norm (L^2, L^∞, etc...) of the target system to conclude on the stability.

Application of the backstepping approach to linear input-delayed dynamical system

What will be of interest for us in the coming developments is that the backstepping approach can be used to study the stability of delayed dynamical systems.

Consider again the simple input-delay system (IV.1). The delayed input can be interpreted as the boundary value of a 1-dimensional transport PDE taking a time D to propagate information injected at the opposite boundary. This translates as

$$\forall\, t \in \mathbb{R}_+ \ , \ \begin{cases} \dot{X}(t) = AX(t) + Bu(0,t) \\ \dfrac{\partial u}{\partial t}(x,t) = \dfrac{1}{D}\dfrac{\partial u}{\partial x}(x,t) \\ u(1,t) = U(t) \end{cases} \tag{IV.8}$$

Leading to the study of a cascaded ODE-PDE system. Upon considering the infinite-dimensional change of coordinates defined by

$$\forall (x,t) \in [0,1] \times \mathbb{R}_+ \ , \ w(x,t) = u(x,t) - \int_0^x k(x,y)u(y,t)\mathrm{d}y - \gamma(x)^T X(t) \tag{IV.9}$$

where $\gamma(\cdot)$ is a given function of x, one can map the system (IV.8) into the target system

$$\forall\, t \in \mathbb{R}_+ \ , \ \begin{cases} \dot{X}(t) = (A+BK)X(t) + Bw(0,t) \\ \dfrac{\partial w}{\partial t}(x,t) = \dfrac{1}{D}\dfrac{\partial w}{\partial x}(x,t) \\ w(1,t) = 0 \end{cases} \tag{IV.10}$$

Remark. Here, the form of $k(\cdot,\cdot)$ and $\gamma(\cdot)$ are obtained by imposing that $w(\cdot,\cdot)$ is a pure transport with velocity D and the boundary conditions are given by the expected form of the ODE. Even though they can be skipped, a good understanding of the basic mechanisms of delayed dynamical system oriented backstepping is preferable for understanding the coming parts of this report.

Applying the computation methods described in paragraph IV.1.2 allows to find the following expression for the control $U(\cdot)$

$$U(t) = u(1,t) = Ke^{AD}X(t) + KD\int_0^1 e^{AD(1-y)}Bu(y,t)\mathrm{d}y = Ke^{AD}X(t) + K\int_{t-D}^t e^{A(D-s)}BU(s)\mathrm{d}s \tag{IV.11}$$

which is exactly the expression obtained for the Smith predictor in section IV.1.1.

In what follows, we will see how this method can be used to study the stability of the more complicated case of a cascaded ODE-PDE system with both input delays and distributed state delays such as the one described by (I.24).

IV.2 Stability analysis of the BHA

The stability analysis of the system of equations (I.24) has been the topic of a recent work by Florent Di Meglio and Delphine Bresch-Pietri, notably in [3]. The main ideas are the same as those presented earlier on, i.e, to design a backstepping transformation which maps the original system to a system which is either stable or convenient to perform a stability analysis using Lyapunov analysis tools.

We shall see however that, even though they developed a proof of stability for the system (I.24) and designed the corresponding control law, it cannot be used straightforwardly due to pratical limitations of the speed of actuator in real systems. This problem called for a wider stability analysis along with additional investigations on how to stabilize this system, the developments of which along with the comprehension of the underlying technical difficulties were one of the main aspects of my work during this internship. But first let us focus on the main general ideas of designing a predictor for general systems that include (I.24).

IV.2.1 General linear input-delayed and distributed state-delayed dynamical system and backstepping transformation

This first part of the stability analysis is a personal reformulation of the work done by Delphine Bresch-Pietri and Florent Di Meglio in their conference article [3]. Understanding and being able to reproduce the technics and concepts developed through this article constituted a rather long part of the beginning of my internship. Besides, having at least a rough understanding of the global approach to study the stability of this class of system is important for the reader in order to understand the associated stability analysis.

Let us consider a linear input-delayed and distributed state-delayed dynamical system of the form

$$\forall\, t \in \mathbb{R}_+ \ , \ \dot{X}(t) = A_0X(t) + A_1\int_{t-D_1(X_t)}^t X(s)\mathrm{d}s + BU(t-D_2) + Ch(t) \tag{IV.12}$$

where $X(\cdot) \in \mathbb{R}^n$, $U(\cdot)$ is a scalar input, $h(\cdot)$ is a disturbance term, $D_1 : \mathcal{C}([-\bar{D},0],\mathbb{R}) \to [0,\bar{D}]$ is a distributed state delay depending on the state history $X_t : s \in [-\bar{D},0] \mapsto X(t+s)$ and $D_2 \in \mathbb{R}_+^*$ is a constant delay.

Similarly, we denote by $X_{t,1} : s \in [-D_1(X_t), 0] \mapsto X(t+s)$ and $U_{t,2} : s \in [-D_2, 0] \mapsto U(t+s)$ the state and control history associated to the delays $D_1(\bullet)$ and D_2.

Remark. It is very important here to understand the notation $X_t(\cdot)$ used for the state history. This notation means that we consider past values of the state $X(\cdot)$ over the time interval $[t - D_1(X_t), t]$.

Remark. To make a connection with the dynamics (I.24) of the BHA, the scalar input $U(\cdot)$ can be for instance $\tilde{\phi}(1,\cdot)$, the constant input delay $D_2 = L_p/c_\phi$ the time taken by the boundary input to propagate down the drillpipes and $D_1(\bullet)$ accounts for $\bar{\tau}_N + \tilde{\tau}_N(\omega_\tau(\cdot))$.

A result of stability for input-delay free dynamical systems

The proof of stability for the general system (IV.12) is grounded on the following result from Pepe & Karafyllis published in 2013 [11] which concerns systems under the same form but with $D_2 = 0$, namely without any input delay.

Theorem 2 (Stability of a linear distributed-state delay system, Pepe & Karafyllis)**.** *There exists $\kappa : \mathcal{C}^0([-D_1, 0], \mathbb{R}) \to \mathbb{R}$ which is a linear and class $\mathcal{C}^1$ feedback law such that the dynamics*

$$\dot{X}(t) = A_0 X(t) + A_1 \int_{t-D_1(X_t)}^{t} X(s)ds + B\kappa(X_{t,1}) + Ch(t) \tag{IV.13}$$

is globally exponentially stable, i.e such that there exists a continuous functional $V_0 : \mathcal{C}^0([-D_1, 0], \mathbb{R}) \to \mathbb{R}$ and three constants C_1, C_2, C_3 such that

$$\forall \phi \in \mathcal{C}^0([-D_1, 0], \mathbb{R}) \ , \ \begin{cases} C_1 \parallel \phi \parallel_{L^\infty(\mathbb{R})} \leq V_0(\phi) \leq C_2 \parallel \phi \parallel_{L^\infty(\mathbb{R})} \\ |\dfrac{\partial V_0}{\partial \phi}(\phi)| \leq C_3 \end{cases}$$

Moreover, the functional $V_0(\bullet)$ is differentiable along the trajectories of (IV.13) *and satisfies $\dot{V}_0(t) \leq -V_0(t)$*

Adaptation to the case of a constant input delay

Knowing this result, our goal is to design a control law for the input delay system (IV.12) that will bring us back to a dynamics of the form (IV.13) using backstepping tools as introduced in the section IV.1.2. The idea will basically be the same as for designing the Smith predictor. Since the control information takes some time to be effective in the system, it is interesting for performance purposes to do a prediction of the future state, which involves some history of the past values of the state over a given time horizon.

Here however, an additional difficulty arises from the fact that the state we try to predict also depends on a distributed state-delay. In the case of *Theorem* 2 where no input delay is considered, the control law does not involve past values $X(\cdot)$ of the state at fixed times but rather past histories $X_{t,1}(\cdot)$ until time t and spanning over time-variable horizons $[t - D_1(X_t), t]$ for any given t.

In our framework, we will need to combine the two notions of prediction and history-based feedback law in order to design a control law stabilizing the system (IV.12) in spite of the input delay D_2.

Let us define now a function $P^t : \tau \in [t - D_2 - \bar{D}, t] \mapsto X(\tau + D_2) \in \mathbb{R}^n$ that will account for a prediction of the state $X(\cdot)$ D_2 time steps ahead. Its analytical expression is given by

$$P^t(\tau) = \begin{cases} X(\tau + D_2) & \text{if } \tau \in [t - D_2 - \bar{D}, t - D_2] \\ e^{A_0(\tau + D_2 - t)} X(t) + \displaystyle\int_t^{\tau + D_2} e^{A_0(\tau + D_2 - s)} Ch(s)\mathrm{d}s & \text{if } \tau \in [t - D_2, t] \\ \qquad + \displaystyle\int_{t-D_2}^{\tau} e^{A_0(\tau - s)} \left[A_1 \int_{s - D_1(P_s)}^{s} P^t(\xi)\mathrm{d}\xi + BU(s) \right] \mathrm{d}s \end{cases} \tag{IV.14}$$

where the expression given for $\tau \in [t - D_2, t]$ originates from the application of a constant-variation formula to $X(\cdot + D_2)$ using (IV.13).

In the framework of *Theorem* 2, the next step would be to build a feedback $\kappa(\bullet)$ taking the state history $X_{t,1}(\cdot)$ as argument. Here however, we will need to replace the history $X_{t,1}(\cdot)$ by the *prediction-history* $P^t_{t,1}(\cdot)$, that is a function that stores values of the prediction $P^t(\cdot)$ over the time interval $[t-D_1(X_t),t]$. The control is then designed by applying the feedback operator $\kappa(\bullet)$ of *Theorem* 2 to the prediction-history $P^t_{t,1}(\cdot)$ rather than the state history $X_{t,1}(\cdot)$.

Remark. Appying the term $\kappa(\bullet)$ to the history $P^t_{t,1}(\cdot)$ instead of $X_{t,1}(\cdot)$ is the operator counterpart of considering a feedback law of the form $KX(\cdot+D)$ instead of $KX(\cdot)$ for a linear input-delayed dynamical system. It is exactly the same principle of saying that one knows a feedback that stabilizes the system with no input delay, builds a corresponding prediction of the state, and then applies this feedback with the prediction rather than the state.

Cascaded ODE-PDE formalism and transport interpretation of delays

As we illustrated it in paragraph IV.1.2, introducing a transport interpretation of the delays allows the use of backstepping transformations and powerful PDE-based tools to design a control law. The corresponding computations being rather heavy, we will not carry them out here (the interested reader can refer to [3] where everything is detailed).

Let us define the distributed variables $\zeta(\cdot,\cdot)$, $\bar{\zeta}(\cdot,\cdot)$ and $u(\cdot,\cdot)$ by

$$\forall (x,t)\in[0,1]\times\mathbb{R}_+\ ,\ \ \zeta(x,t)=X(t+D_1(X_t)(x-1))\ ,\ \bar{\zeta}(x,t)=X(t+\bar{D}(x-1))\ ,\ u(x,t)=X(t+D_2(x-1)) \quad \text{(IV.15)}$$

These variables represent distributed histories of the state $X(\cdot)$ with respect to the delays $D_1(\bullet)$, $\bar{D}$ and D_2 respectively. It then possible to put the system (IV.12) in transport form, interpreting the delayed terms as boundary values of transport PDE satisfied by the previously introduced functions. Up to doing a change of variable in the integral term, the dynamics (IV.12) becomes

$$\begin{cases} \dot{X}(t)=A_0X(t)+A_1D_1(X_{t,1})\displaystyle\int_0^1\zeta(x,t)\mathrm{d}x+Bu(0,t)+Ch(t) \\ D_1(X_{t,1})\dfrac{\partial\zeta}{\partial t}(x,t)=\left(1+\dfrac{\mathrm{d}D_1}{\mathrm{d}X_t}(\dot{X})_t(t)(x-1)\right)\dfrac{\partial\zeta}{\partial x}(x,t) \\ \zeta(1,t)=X(t) \\ D_2\dfrac{\partial u}{\partial t}(x,t)=\dfrac{\partial u}{\partial x}(x,t) \\ u(1,t)=U(t) \end{cases} \quad \text{(IV.16)}$$

One of the main results of [3], in addition to coming up with this intelligent formulation, is to demonstrate that there exists an invertible backstepping transformation mapping the system (IV.16) to the system

$$\begin{cases} \dot{X}(t)=A_0X(t)+A_1D_1(X_{t,1})\displaystyle\int_0^1\zeta(x,t)\mathrm{d}x+Ch(t)+B\kappa_0(\chi(x,\cdot,t))+Bw(0,t) \\ D_1(X_{t,1})\dfrac{\partial\zeta}{\partial t}(x,t)=\left(1+\dfrac{\mathrm{d}D_1}{\mathrm{d}X_t}\dot{X}_t(t)(x-1)\right)\dfrac{\partial\zeta}{\partial x}(x,t) \\ \zeta(1,t)=X(t) \\ D_2\dfrac{\partial w}{\partial t}(x,t)=\dfrac{\partial w}{\partial x}(x,t) \\ w(1,t)=1 \end{cases} \quad \text{(IV.17)}$$

where $\kappa_0(\zeta(\cdot,t))=\kappa(X_{t,1})$, $\chi(\cdot,\cdot,\cdot)$ is a history of the distributed prediction of the state and $w(\cdot,\cdot)$ is the image of $u(\cdot,\cdot)$ through a very sophisticated backstepping transformation that we will not describe here.

The system (IV.17) will be very useful to us for our stability analysis which we shall describe in subsection IV.2.2.

IV.2.2 Lyapunov analysis of the target system

In the paragraph IV.2.1, we have explained how to transform the original dynamical system (IV.12) into the system (IV.17), which will prove much more amenable to stability analyses based on a Lyapunov approach.

In the article [3], a stability analysis is effected for the system (IV.12). However, this analysis does not take into account empirical limitations such as the speed of the actuators used in practice to stabilize oil drilling systems. Moreover, we also consider in this report the additional non-linear friction terms that lead to the arising of the axial limit cycle. These terms are not easy to predict using the tools we saw in what precedes, and are driven by too fast a dynamics for realistic actuators to compensate them.

We are thus going to establish a more general stability property for our system which is based on notions introduced by Eduardo Sontag detailed in [4] : the *Input-to-State Stability* (henceforth noted ISS).

A quick understanding of Input-to-State stability

The notion of Input-to-State Stability is a generalization of the classical notion of *Global Asymptotic Stability* (recalled in [4]) to perturbed systems to deal with the question of robustness of asymptotic stability with respect to disturbances. To formulate the notion in a simple way, a system which is ISS will not be disrupted too much by non-compensated perturbations.

Recall that a dynamical system $\dot{x}(\cdot) = f(x(\cdot), u(\cdot))$ is globally asymptotically stable if and only if there exists a function $\beta(\cdot,\cdot) \in \mathcal{KL}$ such that

$$\forall (x^0, t) \in X \times \mathbb{R}_+ \ , \quad |x(t, x^0)| \leq \beta(|x^0|, t) \tag{IV.18}$$

where a $\mathcal{KL}$ function is a function $\beta : \mathbb{R}_+ \times \mathbb{R}_+ \to \mathbb{R}_+$ such that

$$\begin{aligned} &\forall\, t \in \mathbb{R}_+ \ , \quad \beta(\cdot, t) \in \mathcal{K}_\infty \\ &\forall\, r \in \mathbb{R}_+ \ , \quad \beta(r, t) \underset{t\to\infty}{\downarrow} 0 \end{aligned} \tag{IV.19}$$

and a $\mathcal{K}_\infty$ function is a function $\alpha : \mathbb{R}_+ \to \mathbb{R}_+$ continuous, strictly increasing, unbounded, and such that $\alpha(0) = 0$.

Using the same formalism, a system is said to be ISS with respect to a disturbance $h(\cdot)$ if and only if there exists two functions $(\beta, \gamma) \in \mathcal{KL} \times \mathcal{K}_\infty$ such that

$$\forall (x^0, t) \in X \times \mathbb{R}_+ \ , \quad |x(t, x^0)| \leq \beta(|x^0|, t) + \gamma(\| h \|) \tag{IV.20}$$

where $|\bullet|$ and $\|\bullet\|$ are some norms.

ISS property of the system (IV.17)

Let us now consider again the system (IV.17) obtained from (IV.12) using backstepping tools. We will show that this system is ISS with respect to the disturbance $h(\cdot)$ that is no longer assumed to be compensated by the feedback $\kappa_0(\zeta(\cdot, t))$. The corresponding closed-loop system consequently writes

$$\dot{X}(t) = (A_0 - BK_0)X(t) + Ch(t) + Bw(0, t) \tag{IV.21}$$

where K_0 is chosen such that $(A_0 - BK_0)$ is Hurwitz.

In this framework, we established jointly with Florent Di Meglio the following theorem

Theorem 3 (ISS property of the dynamics of the BHA)**.** *The dynamical system* (IV.12) *is Input-to-State stable with respect to the disturbance $h(\cdot)$, namely there exists a norm $|\bullet|$ as well as two functions $\beta \in \mathcal{KL}$ and $\gamma \in \mathcal{K}_\infty$ such that*

$$\forall\, t \in \mathbb{R}_+ \ , \quad |X(t)| \leq \beta(|X(0)|, t) + \gamma(\| h \|_{L^\infty(\mathbb{R})}) \tag{IV.22}$$

Proof. Our aim here is to obtain an ISS property in L^∞-norm using Lyapunov analysis tools. However, if we consider directly a Lyapunov functional in L^∞-norm, we will lack the differentiability required to prove exponential decay along the trajectories of the closed-loop system. Thus, let us define instead the following L^p-norm based Lyapunov function

$$\forall (p,t) \in \mathbb{N}^* \times \mathbb{R}_+ \ , \quad V_p(t) = \left(\mu_0 - 1 + \frac{1}{2p}\right) V_0^{2p}(X_t) + D_2 b^{2p} \int_0^1 e^{2p\mu_0 D_2 x} w(x,t)^{2p} \mathrm{d}x \tag{IV.23}$$

where $V_0(\bullet)$ is the Lyapunov functional defined in *Theorem* 2 but without the compensation of the disturbance $h(\cdot)$ and where $(b,\mu_0) \in \mathbb{R}_+ \times \mathbb{R}_+$ are tuning parameters for the functional. We impose that $\mu_0 \geq 3$. We will conduct a classical Lyapunov analysis using this functional and then take the limit $p \to \infty$, $p \in \mathbb{N}^*$, to recover a result in term of L^∞-norm.

The function $V_p(\cdot)$ is differentiable along the trajectories of the closed-loop system and its differential writes

$$\begin{aligned}
\dot{V}_p(t) &= \left[2p(\mu_0 - 1) + 1\right] V_0(X_t)^{2p-1} \frac{\partial V_0}{\partial X_t}(X_t).[(A_0 - B_0K)X(t) + Bw(0,t) + Ch(t)] \\
&\quad + D_2 b^{2p} \int_0^1 e^{2p\mu_0 D_2 x} 2p \frac{\partial w}{\partial t}(x,t)\, w(x,t)^{2p-1} \mathrm{d}x \\
&= \left[2p(\mu_0 - 1) + 1\right] V_0(X_t)^{2p-1} \frac{\partial V_0}{\partial X_t}(X_t).[(A_0 - B_0K)X(t) + Bw(0,t) + Ch(t)] \\
&\quad - D_2 b^{2p} w(0,t) - b^{2p} 2p\mu_0 D_2 \int_0^1 e^{2p\mu_0 D_2 x} w(x,t)^{2p} \mathrm{d}x
\end{aligned} \tag{IV.24}$$

recalling that $w(\cdot,\cdot)$ satisfies a transport equation with velocity $\frac{1}{D_2}$ and doing an integration by parts afterwards.

Using the assumptions of *Theorem* 2 we know that

$$\begin{cases}
\dfrac{\partial V_0}{\partial X_t}(X_t).[(A_0 - B_0K)X(t)] \leq -V_0(t) \\
\dfrac{\partial V_0}{\partial X_t}(X_t).[Bw(0,t) + Ch(t)] \leq C_3[Bw(0,t) + Ch(t)]
\end{cases} \tag{IV.25}$$

Moreover, applying the Hölder inequality, one gets

$$\begin{aligned}
2pV_0^{2p-1}(t)\left(\mu_0 - 1 + \frac{1}{2p}\right) C_3[Bw(0,t) + Ch(t)] \leq & (2p-1)V_0^{2p-1}(t) \\
& + \left(\mu_0 - 1 + \frac{1}{2p}\right)^{2p} C_3^{2p} |Bw(0,t) + Ch(t)|^{2p}
\end{aligned} \tag{IV.26}$$

At this point, one can remark that $1 \leq \left(\mu_0 - 1 + \frac{1}{2p}\right) \leq \mu_0$.

Plugging all these intermediate results in (IV.24) one gets

$$\begin{aligned}
\dot{V}_p(t) \leq & \left[-2p(\mu_0 - 2) - 2\right] V_0^{2p}(t) + \mu_0^{2p} C_3^{2p} |Bw(0,t) + Ch(t)|^{2p} \\
& - D_2 b^{2p} w(0,t)^{2p} - b^{2p} 2p\mu_0 D_2 \int_0^1 e^{2p\mu_0 D_2 x} w(x,t)^{2p} \mathrm{d}x
\end{aligned} \tag{IV.27}$$

Let us now deal with the term $A = |Bw(0,t) + Ch(t)|^{2p}$.

$$\begin{aligned}
A &= \sum_{k=0}^{2p} \binom{2p}{k} |Bw(0,t)|^k |Ch(t)|^{2p-k} \\
&\leq \sum_{k=0}^{2p} \binom{2p}{k} \left(\frac{k}{2p} |Bw(0,t)|^{2p} + \frac{2p-k}{2p} |Ch(t)|^{2p}\right) \quad \text{(Hölder inequality)} \\
&= \left[\frac{1}{2p} \sum_{k=0}^{2p} k \binom{2p}{k}\right] |Bw(0,t)|^{2p} + \left[\frac{1}{2p} \sum_{k=0}^{2p} (2p-k) \binom{2p}{k}\right] |Ch(t)|^{2p}
\end{aligned} \tag{IV.28}$$

now let us remark that

$$\begin{cases} \dfrac{1}{2p}\displaystyle\sum_{k=0}^{2p} k\binom{2p}{k} = 2^{2p-1} \\ \dfrac{1}{2p}\displaystyle\sum_{k=0}^{2p} (2p-k)\binom{2p}{k} = 2^{2p} - 2^{2p-1} = 2^{2p-1} \end{cases} \tag{IV.29}$$

And finally

$$[Bw(0,t)+Ch(t)]^{2p} \leq 2^{2p-1}\left(|Bw(0,t)|^{2p} + |Ch(t)|^{2p}\right) \tag{IV.30}$$

One then has the following upper-bound for $\dot{V}_p(\cdot)$

$$\begin{aligned} \dot{V}_p(t) \leq \left[-2p(\mu_0-2)-2\right] V_0^{2p}(t) - \left(D_2 b^{2p} - \frac{\left(2\mu_0 BC_3\right)^{2p}}{2}\right)|w(0,t)|^{2p} \\ + \frac{(2\mu_0|C|C_3)^{2p}}{2}|h(t)|^{2p} - 2p\mu_0 D_2 b^{2p}\int_0^1 e^{2p\mu_0 D_2 x} w(x,t)^{2p}\mathrm{d}x \end{aligned} \tag{IV.31}$$

Since we assumed $\mu_0 \geq 3$ we have also $-2p(\mu_0-2)-2 \leq -2p$ and $-2p\mu_0 \leq -2p$. Moreover, choosing b such that $D_2 b^{2p} - \frac{(2\mu_0 BC_3)^{2p}}{2} \geq 0$ leads to the result

$$\boxed{\dot{V}_p(t) \leq -2pV_p(t) + \frac{(2\mu_0|C|C_3)^{2p}}{2}|h(t)|^{2p}} \tag{IV.32}$$

Taking the constant variation formula on the inequality (IV.32) leads to

$$V_p(t) \leq e^{-2pt}V_p(0) + \frac{(2\mu_0|C|C_3)^{2p}}{2}\int_0^1 |h(s)|^{2p}\mathrm{d}s \leq e^{-2pt}V_p(0) + \frac{(2\mu_0|C|C_3)^{2p}}{2}\parallel h \parallel^{2p}_{L^{2p}(\mathbb{R})} \tag{IV.33}$$

out of positivity of the function $s \mapsto |h(s)|^{2p}$. Moreover, the function $\gamma_p : x \in \mathbb{R}_+ \to \frac{(2\mu_0 CC_3)^{2p}}{2}x^{2p}$ is of class K_∞

Then, one has

$$V_p(t) \leq e^{-2pt}V_p(0) + \gamma_p\left(\parallel h \parallel_{L^{2p}(\mathbb{R})}\right) \tag{IV.34}$$

Leading to

$$V_p(t)^{\frac{1}{2p}} \leq e^{-t}\left(V_p(0) + \gamma_p\left(\parallel h \parallel_{L^{2p}(\mathbb{R})}\right)\right)^{\frac{1}{2p}} \tag{IV.35}$$

Yet, one can easily verify that

$$\left(a^{\frac{1}{2p}} + b^{\frac{1}{2p}}\right)^{2p} = \sum_{k=0}^{2p}\binom{2p}{k}a^{\frac{k}{2p}}b^{\frac{2p-k}{2p}} \geq a+b \tag{IV.36}$$

and also that

$$\forall a,b \in \mathbb{R}_+ \quad \left(a^{\frac{1}{2p}} + b^{\frac{1}{2p}}\right)^{2p} = \sum_{k=0}^{2p}\binom{2p}{k}a^{\frac{k}{2p}}b^{\frac{2p-k}{2p}} \leq \sum_{k=0}^{2p}\binom{2p}{k}\left(\frac{k}{2p}a + \frac{2p-k}{2p}b\right) = 2^{2p-1}(a+b) \tag{IV.37}$$

using (IV.29). Since the function $x \mapsto x^{1/2p}$ is increasing on $\mathbb{R}_+$ and combining with (IV.36) and (IV.37) one has

$$\boxed{\forall a,b \in \mathbb{R}_+ \ , \ (a+b)^{\frac{1}{2p}} \leq \left(a^{\frac{1}{2p}} + b^{\frac{1}{2p}}\right) \leq 2^{\frac{2p-1}{2p}}(a+b)^{\frac{1}{2p}}} \tag{IV.38}$$

Finally, one can use (IV.35) and (IV.38) to obtain

$$\begin{cases} \left(\mu_0 - 1 + \dfrac{1}{2p}\right)^{\frac{1}{2p}} V_0(t) + b_2 \left(D_2 \displaystyle\int_0^1 e^{2p\mu_0 D_2 x} w(x,t)^{2p} \mathrm{d}x \right)^{\frac{1}{2p}} \leq 2 V_p(t)^{\frac{1}{2p}} \\ V_p(t)^{\frac{1}{2p}} \leq e^{-t} \left[\left(\mu_0 - 1 + \dfrac{1}{2p}\right)^{\frac{1}{2p}} V_0(0) + b_2 \left(D_2 \displaystyle\int_0^1 e^{2p\mu_0 D_2 x} w(x,0)^{2p} \mathrm{d}x \right)^{\frac{1}{2p}} + \gamma_p(\left(\| h \|_{L^{2p}(\mathbb{R})} \right)^{\frac{1}{2p}} \right] \end{cases} \tag{IV.39}$$

Hence, recalling the expression of $\gamma_p(\cdot)$, this rewrites

$$\begin{aligned} &\left(\mu_0 - 1 + \frac{1}{2p}\right)^{\frac{1}{2p}} V_0(t) + b_2 \left(D_2 \int_0^1 e^{2p\mu_0 D_2 x} w(x,t)^{2p} \mathrm{d}x \right)^{\frac{1}{2p}} \\ &\leq 2e^{-t} \left[\left(\mu_0 - 1 + \frac{1}{2p}\right)^{\frac{1}{2p}} V_0(0) + b_2 \left(D_2 \int_0^1 e^{2p\mu_0 D_2 x} w(x,0)^{2p} \mathrm{d}x \right)^{\frac{1}{2p}} + 2^{-\frac{1}{2p}} (2\mu_0 |C| C_3) \| h \|_{L^{2p}(\mathbb{R})} \right] \end{aligned} \tag{IV.40}$$

Taking the limit for $p \longrightarrow \infty$ leads to the inequality

$$\boxed{\forall\, t \in \mathbb{R}_+ \ , \ V_0(t) + \max_{x\in[0,1]} \left[e^{\mu_0 D_2 x} w(x,t) \right] \leq e^{-t} \left(V_0(0) + \max_{x\in[0,1]} \left[e^{\mu_0 D_2 x} w(x,0) \right] \right) + 2\mu_0 |C| C_3 \| h \|_{L^\infty(\mathbb{R})}} \tag{IV.41}$$

It is easy to notice that the functions $(x,t) \mapsto e^{-t}x$ and $x \mapsto 2\mu_0|C|C_3 x$ are respectively $\mathcal{KL}$ and $\mathcal{K}_\infty$. Moreover, it can be checked that the function $t \to V_0(t) + \max_{x\in[0,1]} \left[e^{\mu_0 D_2 x} w(x,t) \right]$ is a norm for the state $X(\cdot)$ of the system that also takes into account the control history $U_{\cdot,2}$ with respect to the constant delay D_2. Noting this norm $|\bullet|$, one obtains by (IV.41) the result stated by the theorem.

□

IV.2.3 Consequences of the ISS property on the control design

As it was mentioned earlier on, we conducted the previous ISS analysis since it is not possible for an actuator to exactly compensate terms involving the axial velocity of the BHA. Let us now focus again on our BHA model in order to understand what are the consequences of this result in terms of control design.

Upon expressing $\tilde{\tau}_N(\cdot)$ with the integral term in $\omega(\cdot)$ in both axial and angular dynamics in (I.24), one obtains two equations of the form (IV.12) for the two dynamics where the disturbance terms are linear combinations of the non-linear friction $g(\bullet)$ and a distributed coupling term involving the other state. We thus know that each dynamics is ISS, yet this does not mean that the whole system is stable since the sub-systems are forming a coupled loop and we can only stabilize approximately one of the two.

The notion that could provide us with a closed analytical answer to this question is the one of *Small Gain*. The idea behind it is that if two systems are ISS and coupled in the sense that the state of each system is a perturbation for the other, then controlling only one of the two does not induce any unstability to the other as long as the composition of the two disturbance gains $\gamma_1(\cdot)$ and $\gamma_2(\cdot)$ has a norm lesser or equal to one. We did not manage to prove this statement analytically in our case since evaluating the norm of the disturbances comes down to framing sharply the norms of the non-linear friction and distributed terms, which proved to be too difficult. However, we observed during our simulations that this condition ought to be satisfied since controlling only the angular dynamics of the BHA did not disrupt or visibly modify the axial limit cycle.

Knowing that the system can be controlled only on one of its components without inducing a divergence on the second, we will now describe our control designs for the angular dynamics and their influence on the system.

IV.3 Controller design for the angular velocity of the BHA and numerical implementation

We will now detail the controller designs we made for the system (I.24) using the predictor based approach presented in IV.2.1 and the averaging results obtained in III.2.

We consider the sole angular dynamics written in the form of (IV.12) [1] :

$$\frac{\mathrm{d}\omega}{\mathrm{d}\tau}(\tau) = c_0^{\omega}\left[\tilde{\phi}(1,\tau) - \omega(\tau)\right] + \frac{c_4}{\omega_0}\int_{\tau-\bar{\tau}-\tilde{\tau}_N(\tau)}^{\tau} \omega(s)\mathrm{d}s + h(\tau) \tag{IV.42}$$

where the disturbance term $h(\cdot)$ write

$$\forall \tau \in \mathbb{R}_+ \ , \quad h(\tau) = c_3\lambda\beta g[z(\tau)] - c_3\int_{\tau-\bar{\tau}-\tilde{\tau}_N(\tau)}^{\tau} z(s)\mathrm{d}s \tag{IV.43}$$

The term $\tilde{\phi}(1,\tau) = \tilde{\phi}(0,\tau-D_2) = \tilde{\psi}(0,\tau-D_2) + 2P_{\mathrm{tor}}\tilde{t}_{\mathrm{op}}(\tau-D_2)$ - where $D_2 = \frac{L_p}{t_* c_\phi}$ - is the descending wave input at the rotary table. As described in paragrah I.2.1 and formulated in (I.18) and (I.24), this term is the composition of

- a reflection component proportional to the ascending waves $\tilde{\psi}(0,\cdot)$ propagating in the drillpipes
- a control term $2P_{\mathrm{tor}}\tilde{t}_{\mathrm{op}}(\cdot)$ imposed by the user

As mentioned in section II.2.2, the term that seemed to perturb the most the dynamics of the BHA was the reflection component of $\tilde{\phi}(1,\cdot)$. It was thus mandatory for our controller to compensate both these reflections and the terms of the dynamics (IV.42) preventing exponential stability to obtain a satisfactory convergence to equilibrium.

IV.3.1 Controlling the wave reflections

The control of the reflections occurring at $\chi = 0$ was done rather simply by cancelling the corresponding terms. Some slight algebraic manipulations were required to write this cancellation in a physically plausible form. Indeed, it would not be possible for a user in practice to isolate the component $\tilde{\psi}(0,\cdot)$ but only to measure and act on the total angular velocity $\frac{\tilde{\phi}(0,\cdot)+\tilde{\psi}(0,\cdot)}{2}$.

In the interest of realism, and since the true speed of an actuator is the main practical limitation our whole study revolves around, we took into account the possibility to add an actuator delay to our controller. The different behaviours obtained with this particular feature are displayed along with the other simulation results in IV.3.3.

IV.3.2 Controlling the dynamics of the BHA

In our simulator, we implemented the prediction of the state using (IV.14) but without taking into account the disturbance terms $h(\cdot)$ since building a prediction for them would be prove rather difficult. We thus implemented the following D_2 time steps ahead prediction of $\omega(\cdot)$:

$$P^{\tau}(s) = \begin{cases} \omega(s+D_2) & \text{if} \quad s \in [\tau - D_2 - \bar{D}, \tau - D_2] \\ e^{-c_0^{\omega}(s+D_2-\tau)}\omega(\tau) + \displaystyle\int_{\tau-D_2}^{s} e^{-c_0^{\omega}(s-\xi)}\left[\frac{c_4}{\omega_0}\int_{\xi-\bar{\tau}_N-\tilde{\tau}_N(\xi)}^{\xi} P^{\tau}(\eta)\mathrm{d}\eta + BU(\xi)\right]\mathrm{d}\xi & \text{if} \quad s \in [\tau - D_2, \tau] \end{cases} \tag{IV.44}$$

[1] We recall that the error delay $\tilde{\tau}_N(\cdot)$ is the solution at every time τ of the implicit equation $\displaystyle\int_{\tau-\bar{\tau}_N-\tilde{\tau}_N(\tau)}^{\tau} \omega(s)\mathrm{d}s + \omega_0\tilde{\tau}_N(\tau) = 0$. Plugging this expression of $\tilde{\tau}_N(\cdot)$ in (I.24) allows to put it in the same form as (IV.12).

Remark (1). At some point, we tried to build a prediction for these terms using their previous values based on the argument that the axial dynamics reaches quickly its limit cycle which is quasi-periodic. This method did not yield much results, the impact of the axial terms in the state prediction being of lesser importance than what our controller design already aimed at compensating.

Remark (2). Computing this prediction is by far the costliest part of the simulator due to the presence of the double integral terms that require nested for-loops to be computed.

Recall that the principle of the controller design for a system of the form (IV.12) is to consider a feedback stabilizing the system (IV.42) with zero input-delay and then apply this feedback to the prediction (IV.44) rather than to the state itself.

We then considered different types of feedbacks depending on whether we wanted to compensate only the distributed term in $\omega(\cdot)$ or both the distributed term and the approximate average of the axial disturbance $h(\cdot)$ (see (III.11)). The expressions of the corresponding feedbacks are given by

$$\begin{cases} \kappa\left(P_\tau^\tau(\cdot)\right) = -\dfrac{c_4}{c_0^\omega \omega_0} \displaystyle\int_{\tau-\bar\tau_N-\tilde\tau_N(\tau)}^{\tau} P^\tau(s)\mathrm{d}s & \text{in the first case} \\ \kappa\left(P_\tau^\tau(\cdot)\right) = \dfrac{c_1^\omega}{c_0^\omega \omega_0} \displaystyle\int_{\tau-\bar\tau_N-\tilde\tau_N(\tau)}^{\tau} P^\tau(s)\mathrm{d}s - \dfrac{\Gamma^\omega}{c_0^\omega} & \text{in the second case} \end{cases} \tag{IV.45}$$

where

$$\begin{cases} c_1^\omega = \dfrac{c_3}{(\bar\tau_N+\tau_b)^2}\left[\beta\left(\tau_a+\dfrac{3}{2}\tau_b\right)\left(x_{\lim}-\dfrac{\gamma^z}{c_1^z}\right)-\left(\tau_a+\dfrac{\tau_b}{2}-\dfrac{\tau_a^2}{2\tau_b}\right)x_{\lim}\right] \\ \Gamma^\omega = \dfrac{c_3}{\bar\tau_N+\tau_b}\left[\beta\left(\bar\tau_N-\tau_a-\dfrac{\tau_b}{2}\right)\left(x_{\lim}-\dfrac{\gamma^z}{c_1^z}\right)-x_{\lim}\left(\bar\tau_N-\tau_a+\dfrac{\tau_b}{2}+\dfrac{\tau_a^2}{2\tau_b}\right)\right]+c_4\bar\tau_N \end{cases} \tag{IV.46}$$

These expressions are obtained by remarking that in the absence of the input delay D_2, the feedbacks given by (IV.45) applied to $\omega(\cdot)$ would make the system (IV.42) exponentially stable modulo the disturbance term $h(\cdot)$. The constants c_1^ω and Γ^ω are obtained by plugging (III.11) into (IV.42) and applying the same compensation technique to the resulting terms in $\tilde\tau_N(\cdot)$.

IV.3.3 Closed-loop simulations of the system

Now that we justified and presented our controller design, let us have a look at some simulation results using the different types of feedbacks introduced in Section IV.3. Let it be noted that the plots are displayed here in the re-scalled physical variables and that the angular boundary conditions at $x = 0$ are torque conditions corresponding to the physical equation (I.5).

Remark. The control-free angular velocity of the BHA can be observed in figure IV.4. It was not displayed here for the sake of clarity.

Figure IV.2 calls for some comments :

- ◇ As mentioned before at several occasions, this figure illustrates the fact that once the angular reflections occurring at $x = 0$ are removed, the torsional dynamics is much more stable, entering a small-amplitude limit cycle which is drifted away by a constant value from the equilibrium $\Omega_0 = 120$ Rev/min.
- ◇ The remaining oscillations share the same pace as the axial dynamics. They are the remaining part of the disturbances we could not compensate due to the speed limitation of the actuator.
- ◇ The compensation of the distributed term in $\omega(\cdot)$ and of the approximate averages of the axial disturbances $h(\cdot)$ proves efficient in moving the torsional limit cycle toward Ω_0.

The results displayed in figure IV.2 are rather satisfactory : the torsional dynamics is nearly stabilized and the more accurate the controller design the closest the final limit cycle is to the equilibrium. However, further simulations results have shown that our controller design was still at odds with the empirical limitations of the system. Indeed we observed that the controller was still acting to quickly compared to

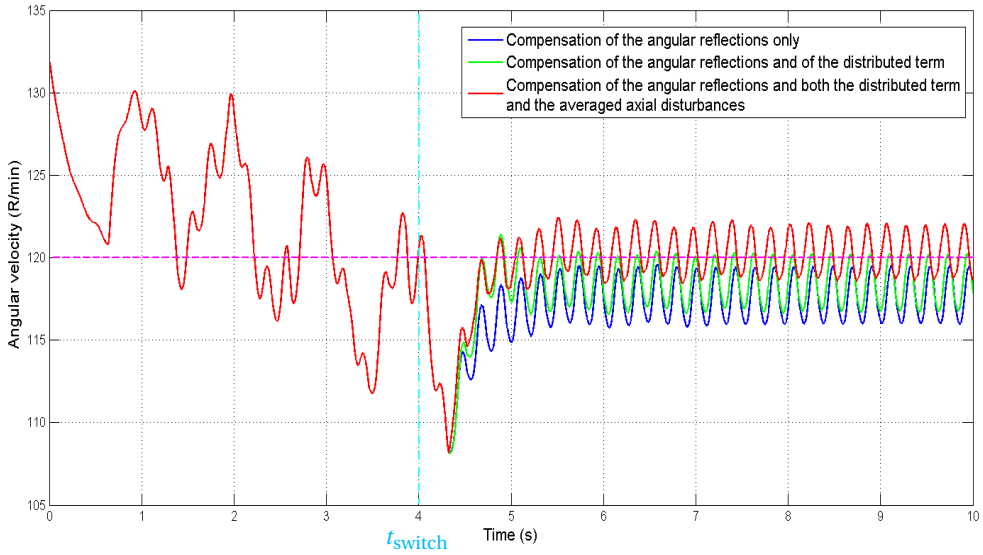

Figure IV.2: *Plots of the angular velocity of the BHA (in revolutions per minute) for $t \in [0,10]$ after applying the different control strategies detailed in section IV.3 and turning the controller on at time $t_{switch} = 4s$.*

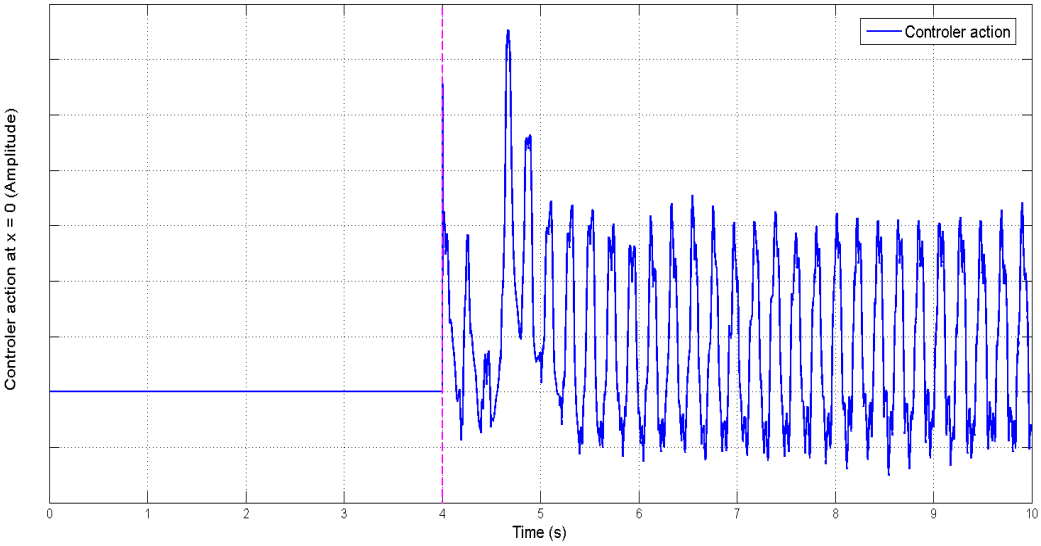

Figure IV.3: *Plot of the torque control applied by the actuator at $x = 0$*

what a realistic actuator could do in practice. In figure IV.3, it can be seen that the pace of the controller is analogous to the one of the axial dynamics as displayed for instance in figure II.5.

This is unsatisfactory given the fact that we wanted to design a slow-pace controller. This issue can be dealt with by taking into account the dynamics of the actuator. In a simple approximation, this dynamics can be modeled as a low-pass filter of time constant T_{ac} applied to the controller. The simulation results in figure IV.4 - obtained by taking $T_{\text{ac}} = t_* \simeq 2.2051s$ - show the angular velocity of the BHA after applying the same control strategies as in figure IV.2 and turning the controller on at $t_{\text{switch}} = 3.75s$.

It can be seen in figure IV.4 that even though the actuator dynamics blurs out the differences of performance between the controller, all of them lead to a limit cycle oscillating around Ω_0. It can be noticed as well that the best controller (red) brings the average of the limit cycle slightly closer to Ω_0 than the simplest one (blue).

These limit cycles are much cruder and present a bigger amplitude than in the case of an arbitrarily fast actuator as illustrated in figure IV.2, yet they still provide us with an almost stabilized dynamics. It can be noted that a time constant of roughly 2 seconds seems still rather fast for an industrial oil drilling actuator. One can obtain more realistic results upon taking bigger values for T_{ac}. This may lead however to the loss of the limit cycle behaviour the we observed in figures IV.2 and IV.4.

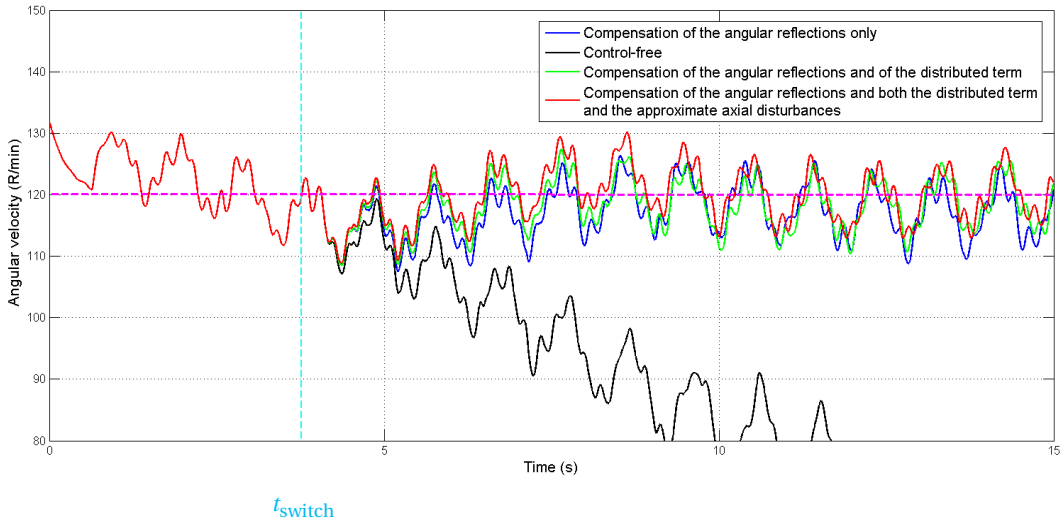

Figure IV.4: *Plots of the angular velocity of the BHA (in revolutions by minute) for $t \in [0,15]$ after applying the different control strategies detailed in section IV.3, composed with an actuator dynamics of time constant $T_{ac} = t_*$.*

We display in figure IV.5 the behaviour of the angular velocity of the BHA upon considering a time constant $T_{\text{ac}} = 4\,t_*$ for the actuator dynamics and

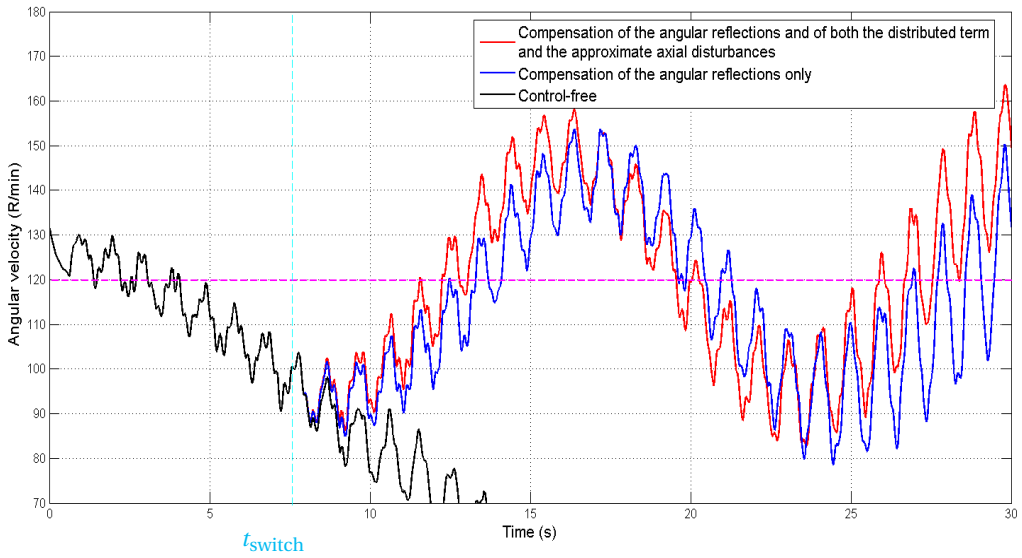

Figure IV.5: *Plots of the angular velocity of the BHA (in revolutions by minute) for $t \in [0,30]$ after applying the different control strategies detailed in section IV.3, composed with an actuator dynamics of time constant $T_{ac} = 4\,t_*$.*

We see here that the limit cycle behaviour is lost and that the velocity is most likely to diverge due to the increasing magnitude of the oscillations. The controller which effects are displayed in red seems to tame lightly the increase of the amplitude of the oscillations compared to the simpler controller in blue, but follows a diverging behaviour all the same.

In conclusion, the controller design presented in this chapter is theoretically satisfactory and practically efficient upon considering actuator dynamics that are either arbitrarily fast or that have a sufficiently small characteristic time. The effect of stabilizing only the angular dynamics of the system does not however lead to a stabilization of the axial dynamics. The axial stick-slip cycle remains essentially unchanged in each of the cases displayed in figures IV.2, IV.4 and IV.5 corresponding to the control of the torsional dynamics. Empirically, the better the stabilization of the torsional dynamics the closest the average of the axial cycle is to its nominal value, but the difference from one controller to the other remains very small.

Conclusion

During this internship, we approached the problem of stabilizing the dynamics of a rotary oil drilling system in a rather new way. The introduction of the non-linear friction terms inducing the stick-slip behaviours in a backstepping-based control framework is innovative and presents along with the considerations linked to the speed of the actuators the main contribution of this internship. In this framework, we adapted the results of recent work done in [3] to obtain a more general stability result for our system, taking into account the non-linear and fast-acting disturbances, and described the corresponding controller design. A more accurate model for the actuator dynamics, an analytical demonstration of the Small Gain Theorem that appears to apply to our system and the design of a more intelligent controller acting partly on the axial dynamics would be interesting directions for further work.

The implementation of a modular and pliant simulator to exhibe the corresponding results also was a wide part of my work, as mentioned earlier as most of the remarks made in II.1.2 are stemmed from experimented methods.

We conducted in parallel of this main study smaller ones that did not lead to much breakthroughs. We tried for instance to analyse the robustness margins of the Smith predictor applied to linear autonomous input-delayed systems, using both classical complex variables results - Nyquist diagrams, see appendix B - and recent backstepping tools developped by Florent Di Meglio's PhD student Jean Auriol. We also dug into the practical particularities of simulating a distributed BHA model and coded the corresponding solver. We obtained results fairly identical qualitatively speaking to those displayed in [1].

This internship was very instructive for me professionally speaking. It allowed me to learn more about what I seak in terms of research topics and environment and gave me the opportunity to work on a very interesting subject which was foreign to me in the first place.

Appendix A

Axial stick-slip cycle analysis : computations details

In this appendix, we give further details on the piecewise computation of the solution to the axial stick-slip dynamics discussed in section **??** and described by the equations (III.3).

Let us now focus on each phase in more detail.

A.1 Phase b

This phase is the first to consider since its solution is used in phase a through the delayed terms.

Here, the systems follows the dynamic

$$\begin{aligned} \dot{x}_b(\tau) &= z_b(\tau) \\ \dot{z}_b(\tau) &= -c_0^z z_b(\tau) - c_1 x_b(\tau) + \gamma \end{aligned} \tag{A.1}$$

or equivalently

$$\ddot{x}_b(\tau) + c_0^z \dot{x}_b(\tau) + c_1 x_b(\tau) = \gamma \tag{A.2}$$

since $c_0^z \simeq 12.4$ and $c_1 \simeq 3.10^3$ in practice, one can define $\underline{-\Delta = (c_0^z)^2 - 4c_1 < 0}$ (we keep the notation Δ throughout this report for simplicity) leading to the solution

$$\forall \tau \in [\tau_a, \tau_a + \tau_b] \ , \ \begin{cases} x_b(\tau) = e^{-\frac{c_0^z}{2}\tau}\left[\lambda_b \cos\left(\frac{1}{2}\sqrt{\Delta}\tau\right) + \mu_b \sin\left(\frac{1}{2}\sqrt{\Delta}\tau\right)\right] + \frac{\gamma}{c_1} \\ x_b(\tau_a + \tau_b) = x_{\lim} \\ \dot{x}_b(\tau_a + \tau_b) = 0 \end{cases} \tag{A.3}$$

Here analytical expressions can be obtained for (λ_b, μ_b) as functions of $x_{\lim}$, τ_a and τ_b :

$$\begin{cases} \lambda_b = e^{\frac{c_0^z}{2}(\tau_a+\tau_b)}\left[\cos\left(\frac{1}{2}\sqrt{\Delta}(\tau_a+\tau_b)\right) - \frac{c_0^z}{\sqrt{\Delta}}\sin\left(\frac{1}{2}\sqrt{\Delta}(\tau_a+\tau_b)\right)\right]\left(x_{\lim} - \frac{\gamma}{c_1}\right) \\ \mu_b = e^{\frac{c_0^z}{2}(\tau_a+\tau_b)}\left[\frac{c_0^z}{\sqrt{\Delta}}\cos\left(\frac{1}{2}\sqrt{\Delta}(\tau_a+\tau_b)\right) + \sin\left(\frac{1}{2}\sqrt{\Delta}(\tau_a+\tau_b)\right)\right]\left(x_{\lim} - \frac{\gamma}{c_1}\right) \end{cases} \tag{A.4}$$

After some algebraic simplifications the following expression is obtained for $x_b(\tau)$

$$\boxed{\forall \tau \in [\tau_a, \tau_a + \tau_b] \ , \ x_b(\tau) = \frac{\gamma}{c_1} + \left(x_{\lim} - \frac{\gamma}{c_1}\right) e^{-\frac{c_0^z}{2}(\tau - \tau_a - \tau_b)}\left[\cos\left(\frac{1}{2}\sqrt{\Delta}(\tau - \tau_a - \tau_b)\right) + \frac{c_0^z}{\sqrt{\Delta}}\sin\left(\frac{1}{2}\sqrt{\Delta}(\tau - \tau_a - \tau_b)\right)\right]} \tag{A.5}$$

A.2 Phase a

Here, the system is still in a slip-phase, but now the delayed position $x(\tau - \tau_N)$ is of the same form as in (A.5) but with the boundary conditions

$$\tilde{x}_b(\tau_a) = \dot{\tilde{x}}_b(\tau_a) = 0 \tag{A.6}$$

In a word, $\tilde{x}_b(\cdot)$ is a translated version of $x_b(\cdot) : \forall \tau \in \mathbb{R}_+ \ , \ \tilde{x}_b(\tau) = x_b(\tau + \tau_b) - x_{\text{lim}}$. Hence

$$\boxed{\forall \tau \in [0, \tau_a] \ , \ \tilde{x}_b(\tau) = \left(\frac{\gamma}{c_1} - x_{\text{lim}}\right)\left(1 - e^{-\frac{c_0^z}{2}(\tau - \tau_a)}\left[\cos\left(\frac{1}{2}\sqrt{\Delta}(\tau - \tau_a)\right) + \frac{c_0^z}{\sqrt{\Delta}}\sin\left(\frac{1}{2}\sqrt{\Delta}(\tau - \tau_a)\right)\right]\right)} \tag{A.7}$$

The dynamics is thus given by

$$\ddot{x}_a(\tau) + c_0^z \dot{x}_a(\tau) + c_1 x_a(\tau) = \gamma + c_1 \tilde{x}_b(\tau) \tag{A.8}$$

leading to the expression for the solution

$$\forall \tau \in [0, \tau_a] \ , \ \begin{cases} x_a(\tau) = e^{-\frac{c_0^z}{2}\tau}\left[\lambda_a \cos\left(\frac{1}{2}\sqrt{\Delta}\tau\right) + \mu_a \sin\left(\frac{1}{2}\sqrt{\Delta}\tau\right)\right] \\ \qquad\qquad + \dfrac{2}{\sqrt{\Delta}}\displaystyle\int_0^\tau e^{-\frac{c_0^z}{2}(\tau - s)} \sin\left(\frac{1}{2}\sqrt{\Delta}(\tau - s)\right)\left[\gamma + c_1 \tilde{x}_b(s)\right] \mathrm{d}s \\ x_a(\tau_a) = x_b(\tau_a) \\ \dot{x}_a(\tau_a) = \dot{x}_b(\tau_a) \end{cases} \tag{A.9}$$

where the two conditions in $\tau = \tau_a$ are junction conditions.

It can be noted here that the limit cycle condition on x_a is

$$x_a(0) = \dot{x}_a(\tau) = 0 \tag{A.10}$$

which enables to remark that

$$\lambda_a = 0 \ , \ \mu_a = 0 \tag{A.11}$$

Then, one has

$$\forall \tau \in [0, \tau_a] \ , \ x_a(\tau) = \frac{2}{\sqrt{\Delta}} \int_0^\tau e^{-\frac{c_0^z}{2}(\tau - s)} \sin\left(\frac{1}{2}\sqrt{\Delta}(\tau - s)\right)\left[\gamma + c_1 \tilde{x}_b(s)\right] \mathrm{d}s \tag{A.12}$$

Since $\tilde{x}_b(\tau)$ is given by (A.7), it follows that

$$\begin{aligned} x_a(\tau) = & \frac{4\gamma - 2c_1 x_{\text{lim}}}{\sqrt{\Delta}} \int_0^\tau e^{-\frac{c_0^z}{2}(\tau - s)} \sin\left(\frac{1}{2}\sqrt{\Delta}(\tau - s)\right) \mathrm{d}s \\ & - \frac{2(\gamma - c_1 x_{\text{lim}})}{\sqrt{\Delta}} e^{-\frac{c_0^z}{2}(\tau - \tau_a)} \int_0^\tau \sin\left(\frac{1}{2}\sqrt{\Delta}(\tau - s)\right) \cos\left(\frac{1}{2}\sqrt{\Delta}(s - \tau_a)\right) \mathrm{d}s \\ & - \frac{2c_0^z(\gamma - c_1 x_{\text{lim}})}{\Delta} e^{-\frac{c_0^z}{2}(\tau - \tau_a)} \int_0^\tau \sin\left(\frac{1}{2}\sqrt{\Delta}(\tau - s)\right) \sin\left(\frac{1}{2}\sqrt{\Delta}(s - \tau_a)\right) \mathrm{d}s \end{aligned} \tag{A.13}$$

where

$$\begin{cases} \displaystyle\int_0^\tau \sin\left(\frac{1}{2}\sqrt{\Delta}(\tau-s)\right)\cos\left(\frac{1}{2}\sqrt{\Delta}(s-\tau_a)\right)\mathrm{d}s = \frac{1}{\sqrt{\Delta}}\sin\left(\frac{1}{2}\sqrt{\Delta}\tau\right)\sin\left(\frac{1}{2}\sqrt{\Delta}\tau_a\right)+\frac{\tau}{2}\sin\left(\frac{1}{2}\sqrt{\Delta}(\tau-\tau_a)\right) \\ \displaystyle\int_0^\tau \sin\left(\frac{1}{2}\sqrt{\Delta}(\tau-s)\right)\sin\left(\frac{1}{2}\sqrt{\Delta}(s-\tau_a)\right)\mathrm{d}s = \frac{1}{\sqrt{\Delta}}\sin\left(\frac{1}{2}\sqrt{\Delta}\tau\right)\cos\left(\frac{1}{2}\sqrt{\Delta}\tau_a\right)-\frac{\tau}{2}\cos\left(\frac{1}{2}\sqrt{\Delta}(\tau-\tau_a)\right) \\ \displaystyle\int_0^\tau e^{-\frac{c_0^z}{2}(\tau-s)}\sin\left(\frac{1}{2}\sqrt{\Delta}(\tau-s)\right)\mathrm{d}s = \frac{\sqrt{\Delta}}{2c_1}\left(1-e^{-\frac{c_0^z}{2}\tau}\left[\cos\left(\frac{1}{2}\sqrt{\Delta}\tau\right)+\frac{c_0^z}{\sqrt{\Delta}}\sin\left(\frac{1}{2}\sqrt{\Delta}\tau\right)\right]\right) \end{cases} \tag{A.14}$$

This altogether leads to the following expression for $x_a(\tau)$

$$\begin{aligned} x_a(\tau) = {} & \left(2\frac{\gamma}{c_1}-x_{\lim}\right)\left(1-e^{-\frac{c_0^z}{2}\tau}\left[\cos\left(\frac{1}{2}\sqrt{\Delta}\tau\right)+\frac{c_0^z}{\sqrt{\Delta}}\sin\left(\frac{1}{2}\sqrt{\Delta}\tau\right)\right]\right) \\ & -\frac{2c_1}{\Delta}\left(\frac{\gamma}{c_1}-x_{\lim}\right)e^{-\frac{c_0^z}{2}(\tau-\tau_a)}\sin\left(\frac{1}{2}\sqrt{\Delta}\tau\right)\left[\sin\left(\frac{1}{2}\sqrt{\Delta}\tau_a\right)+\frac{c_0^z}{\sqrt{\Delta}}\cos\left(\frac{1}{2}\sqrt{\Delta}\tau_a\right)\right] \\ & -\frac{\tau c_1}{\sqrt{\Delta}}\left(\frac{\gamma}{c_1}-x_{\lim}\right)e^{-\frac{c_0^z}{2}(\tau-\tau_a)}\left[\sin\left(\frac{1}{2}\sqrt{\Delta}(\tau-\tau_a)\right)-\frac{c_0^z}{\sqrt{\Delta}}\cos\left(\frac{1}{2}\sqrt{\Delta}(\tau-\tau_a)\right)\right] \end{aligned} \tag{A.15}$$

A.3 Junction condition between phases a and b

For the study of the slip-phase, there remains to study the junction conditions of the two solutions at $\tau=\tau_a$ which read in explicit form :

$$\begin{cases} \dfrac{\gamma}{c_1}+\left(x_{\lim}-\dfrac{\gamma}{c_1}\right)e^{\frac{c_0^z}{2}\tau_b}\left[\cos\left(\frac{1}{2}\sqrt{\Delta}\tau_b\right)-\frac{c_0^z}{\sqrt{\Delta}}\sin\left(\frac{1}{2}\sqrt{\Delta}\tau_b\right)\right] = \left(2\dfrac{\gamma}{c_1}-x_{\lim}\right)\left(1-e^{-\frac{c_0^z}{2}\tau_a}\left[\cos\left(\frac{1}{2}\sqrt{\Delta}\tau_a\right)+\frac{c_0^z}{\sqrt{\Delta}}\sin\left(\frac{1}{2}\sqrt{\Delta}\tau_a\right)\right]\right) \\ \qquad\qquad +\left(\dfrac{\gamma}{c_1}-x_{\lim}\right)\left(\dfrac{c_0^z c_1\tau_a}{\Delta}-\dfrac{2c_1}{\Delta}\left[\sin\left(\frac{1}{2}\sqrt{\Delta}\tau_a\right)^2+\frac{c_0^z}{2\sqrt{\Delta}}\sin\left(\sqrt{\Delta}\tau_a\right)\right]\right) \\ 2\left(x_{\lim}-\dfrac{\gamma}{c_1}\right)e^{\frac{c_0^z}{2}\tau_b}\sin\left(\frac{1}{2}\sqrt{\Delta}\tau_b\right)+2\left(2\dfrac{\gamma}{c_1}-x_{\lim}\right)e^{-\frac{c_0^z}{2}\tau_a}\sin\left(\frac{1}{2}\sqrt{\Delta}\tau_a\right) = \left(\dfrac{\gamma}{c_1}+x_{\lim}\right)\dfrac{(2c_1\tau_a-c_0^z)}{\Delta} \\ \qquad\qquad +\left(\dfrac{\gamma}{c_1}-x_{\lim}\right)\left[\sin\left(\frac{1}{2}\sqrt{\Delta}\tau_a\right)+\frac{c_0^z}{\sqrt{\Delta}}\cos\left(\frac{1}{2}\sqrt{\Delta}\tau_a\right)\right]\left[\cos\left(\frac{1}{2}\sqrt{\Delta}\tau_a\right)-\frac{c_0^z}{\sqrt{\Delta}}\sin\left(\frac{1}{2}\sqrt{\Delta}\tau_a\right)\right] \end{cases}$$

A.4 Phase c

The system enters a stick-phase corresponding to

$$\forall\tau\in[\tau_a+\tau_b,\tau_N]\ ,\ \ddot{x}_c(\tau)=0\ ,\ \dot{x}_c(\tau)=0\ ,\ x_c(\tau-\tau_N)=0\ ,\ x_c(\tau)=x_{\lim} \tag{A.16}$$

which leads to the following expression for g :

$$\boxed{\forall\tau\in[\tau_a+\tau_b,\tau_N]\ ,\ g=\frac{1}{\lambda}\left(x_{\lim}-\frac{\gamma}{c_1}\right)} \tag{A.17}$$

A.5 Phase d and e

The system exits the phase c and enters the phase d when τ reaches τ_N. Then, the delayed state $x(\tau-\tau_N)$ is not equal to 0 anymore but is defined by $x_d(\tau-\tau_N)=\tilde{x}_a^s(\tau)$, where $\tilde{x}_a^s(\tau)$ is of the form (A.15) with the boundary conditions

$$\tilde{x}_a^s(\tau_N)=\dot{\tilde{x}}_a^s(\tau_N)=0 \tag{A.18}$$

In this case, g is defined by

$$\boxed{\forall \tau \in [\tau_N, \tau_N + \tau_a] \ , \ g = \frac{1}{\lambda}\left(x_{\text{lim}} - \tilde{x}_a^s(\tau) - \frac{\gamma}{c_1}\right)} \tag{A.19}$$

Similarly, one defines $\tilde{x}_b^s(\tau)$ as a solution of the dynamic (A.2) but with the boundary conditions

$$\tilde{x}_b^s(\tau_N + \tau_a) = \tilde{x}_a^s(\tau_N + \tau_a) \ , \ \dot{\tilde{x}}_b^s(\tau_N + \tau_a) = \dot{\tilde{x}}_a^s(\tau_N + \tau_a) \tag{A.20}$$

On this final interval, g is given by

$$\boxed{\forall \tau \in [\tau_N + \tau_a, \tau_N + \tau_b] \ , \ g = \frac{1}{\lambda}\left(x_{\text{lim}} - \tilde{x}_b^s(\tau) - \frac{\gamma}{c_1}\right)} \tag{A.21}$$

A.6 Characterizing the end of the stick-phase

The end of the stick-phase is characterized in [5]. by the equation

$$g\left[\dot{x}(\tau_N + \tau_q)\right] = 0 \tag{A.22}$$

where τ_q is a parameter that depends on τ_a and τ_b in a way that we shall explain right now.

In [5], it is considered that $\tau_b > \tau_a$. With our model, if we define all the parameters as they did, τ_a may be larger or equal than τ_b in some cases depending on the constant input u involved in the expression of γ. This does not invalidate our study since, for values of $\tau_a \geq \tau_b$ but close to τ_b - which occurs in practice -, the analytical solution of the equations characterizing the limit cycle still yields good results as displayed in figures IV.2 and IV.4. However, if τ_a becomes significantly larger than τ_b, the model may lose its validity.

We shall consider further on that the system always exits the stick-phase at $\tau_N + \tau_b$, i.e. $\tau_q = \tau_b$. Another idea could be to consider that the system exits the stick-phase at time $\tau_N + \tau_b$.

Appendix B

Robustness margins of the Smith predictor

B.1 Overview and analysis of a particular case

As we have illustrated in the section IV.1 , the prediction-based approach to stabilizing a delay system is way more efficient in terms of performance than a classical feedback approach. However, in order to design a Smith predictor in the same fashion as we have juste seen, one requires perfect (or at least good) knowledge of the delay D of the system, which in practice may be inaccesible. Indeed, using an inaccurately estimated delay D to design a Smith predictor can lead to heavy losses in performance and stability and possibly create an unstable closed-loop system. Thus, the evolution of the robustness margins and of the stability of the closed-loop system involving a Smith predictor with respect to delay mismatchs is a very interesting information to get.

However, obtaining this kind of information analytically is quite complicated. Our aim here is only to give a small (but hopefully clear) illustration of the sensitivity of the Smith predictor with respect to delay mismatches through simulations on simple linear systems.

Consider again the scalar example given in (IV.4) but with $D = 0.1$ being the true delay and D_0 the estimated delay. This simple example of unstable first order system will be sufficient to highlight most of the responses to both traditional and Smith predictor controllers to delay mismatches, as illustrated on the figures B.1 and B.2.

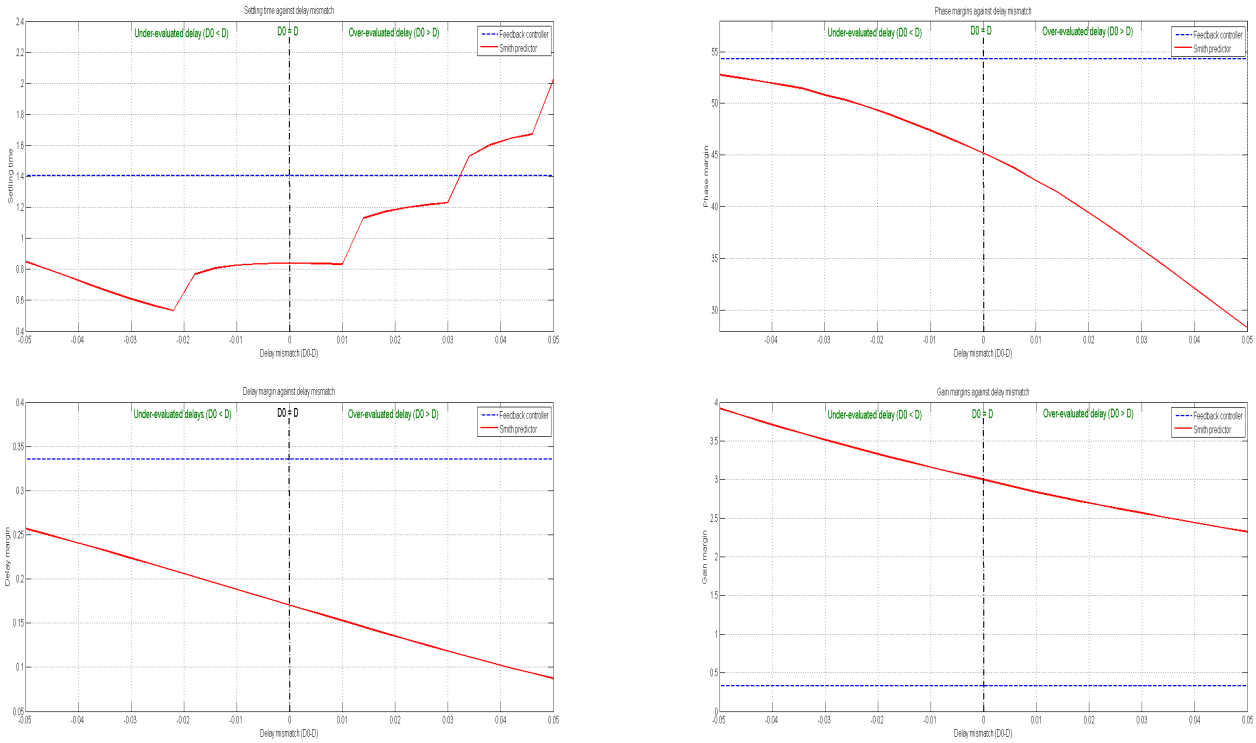

Figure B.1: *Graphical comparisons between a classical feedback and a Smith predictor in the case of delay mismatches*

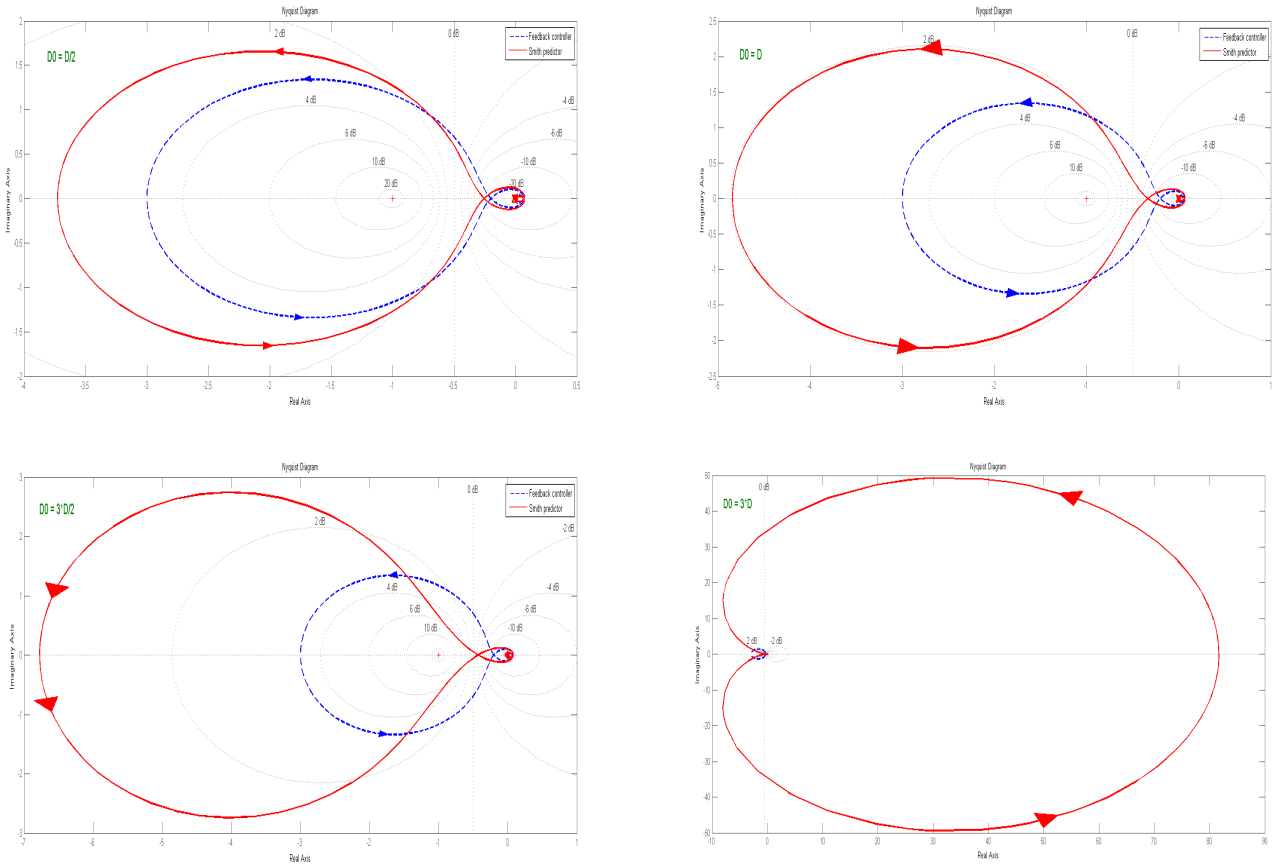

Figure B.2: *Nyquist diagrams corresponding to relevant values of the delay mismatche considered in our analysis :* $D_0 \in \{\frac{D}{2}, D, \frac{3D}{2}, 3D\}$

These figures suggest the following conjectures concerning the Smith predictor :

- A Smith predictor performs much better than a linear feedback provided the delay governing the dynamics of the system is well estimated

- Underestimating the delay seems generally less harmful than overestimating it (see the left part of the four diagrams in figure B.1). Both the performance and the robustness margins seem in this case slightly better than when the delay is fully known.

B.2 Improving the Smith predictor's robustness

We saw that, overall, the Smith predictor may lack robustness compared to a classical feedback controller. We thus tried to play around with its expression to try and get a more robust form of controller.

Even though our two attempts in this direction did not yield any results, I would like to briefly present the main underlying concepts since they may present interesting ideas are still open questions.

The two approaches are mainly based on the same notion which we will now explain. Consider the classical (developed) form of a Smith predictor :

$$U(t) = KX(t+D) = K\left(e^{AD}X(t) + \int_{t-D}^{t} e^{A(t-s)}BU(s)\mathrm{d}s\right) \tag{B.1}$$

An inference drawn by Florent Di Meglio while working on this question was that the lack of robustness may arise from the weak dependancy of the controller with respect to the state $X(\cdot)$. Indeed, the prediction term only involves past-values of the control. Hence, our idea was to try to modify this expression in order to have a more significant dependence in $X(\cdot)$ in the controller.

B.2.1 Fully replacing the dependence in U with a dependence in X

We first tried to consider the integral term in (B.1) as a Kernel integral of the form

$$U(t) = K\left(e^{AD}X(t) + \int_0^t G(t-s)U(s)\mathrm{d}s\right) \quad \text{where} \quad G(s) = \mathbb{1}_{[0,D]}(s)e^{As}B \tag{B.2}$$

Considering this equation a depending on the unknown $U(\cdot)$, it is an Volterra-integral equation of the second kind in convolution form since the Kernel depends of the difference $(t-s)$.

The form of the solution to these equations is well known and writes

$$U(t) = K\left(e^{AD}X(t) + \int_0^t H(t,s)X(s)\mathrm{d}s\right) \tag{B.3}$$

It is possible to find a solution for this equation by injecting (B.3) in (B.2) which leads to another Volterra equation whose unknown is $H(\cdot,\cdot)$.

Even though it yields some results, this method presents an important drawback. Indeed, one will have to store a non-fixed and increasing number of values of the state $X(\cdot)$ as t increases to compute the control $U(\cdot)$. This makes this approach much inconvenient and inefficient for any kind of numerical implementation.

B.2.2 Introducing more dependence in X

Another idea we thought would lead to involve more of the history of the state $X(\cdot)$ into the design of the controller was to inject the implicit expression (B.1) in $U(\cdot)$ in itself, namely

$$\begin{aligned}
U(t) &= K\left(e^{AD}X(t) + \int_{t-D}^t e^{A(t-s)}BU(s)\mathrm{d}s\right) \\
&= K\left(e^{AD}X(t) + \int_{t-D}^t e^{A(t-s)}B\left[e^{AD}X(s) + \int_{s-D}^s e^{A(s-\xi)}BU(\xi)\mathrm{d}\xi\right]\mathrm{d}s\right) \\
&= K\left(e^{AD}X(t) + \int_{t-D}^t e^{AD}X(s) + \left[\int_s^t e^{A(t-\xi)}Be^{A(\xi-s)}\mathrm{d}\xi\right]BU(s)\mathrm{d}s + \int_{t-2D}^{t-D}\left[\int_{t-2D}^{s+D} e^{A(t-\xi)}Be^{A(\xi-s)}\mathrm{d}\xi\right]BU(s)\mathrm{d}s\right)
\end{aligned} \tag{B.4}$$

One can see that now, the controller involves values of the state over the time period $[t-D, t]$ and values of the controle over $[t-2D, t-D]$.

However, upon taking the Laplace transformation of this expression and going through some algebraic simplifications, one finds the same transfer function between $U(\cdot)$ and $X(\cdot)$ as in the case of the simple Smith predictor (B.1) (see [7] for instance). This procedure, even though meaningful in terms of dependence of the control relatively to the state, does not yield a stronger robustness.

Bibliography

[1] C. Germay, V. Denoël, and E. Detournay. Multiple mode analysis of the self-excited vibrations of rotary drilling systems. *Journal of Sound and Vibrations*, 2009.

[2] M. Krstic and D. Bresch-Pietri. Adaptive output-feedback for wave pde with anti-damping – application to surface-based control of oil drilling stick-slip instability. *Conference on Decision and Control*, 2014.

[3] F. Di Melgio and D. Bresch-Pietri. Prediction-based control of linear input-delay system subject to state-dependent state delay – application to suppression of mechanical vibrations in drilling. *2nd IFAC Workshop on Control of systems governed by Partial Differential Equations (Invited session)*, 2016.

[4] E. D. Sontag. Input to state stability : Basic concepts and results. http://web.mit.edu/~esontag/www/FTP_DIR/04cetraro.pdf.

[5] N. Van de Wouw B. Besselink and H. Nijmeijer. A semi-analytical study of stick-slip oscillations in drilling systems. *Journal of Computational and Nonlinear Dynamics*, 2011.

[6] Smith O.J.M. Closer control of loops with dead time. *Chemical Engineering Progress*, 1957.

[7] D. Bresch-Pietri. Robust control of variable time-delay systems. theoretical contributions and applications to engine control. https://pastel.archives-ouvertes.fr/pastel-00803271/document, 2012.

[8] M. Krstic and A. Smyshlyaev. Closed form boundary state feedbacks for a class of 1d partial integro-differential equations. *IEEE Transactions on Automatic Control 49*, 2004.

[9] M. Krstic and A. Smyshlyaev. Backstepping observers for a class of parabolic pdes 54. *Systems and Control Letters*, 2005.

[10] M. Krstic and A. Smyshlyaev. *Boundary Control of PDEs : A Course on Backstepping Design*. SIAM, 2008.

[11] P. Pepe and I.Karafyllis. Converse lyapunov–krasovskii theorems for systems described by neutral functional differential equations in hale's form. *International Journal of Control*, 2013.